AGU100 ADVANCING EARTH AND SPACE SCIENCE

Earth and Space Science

RESEARCH ARTICLE
10.1029/2019EA000693

Special Section:
Results from the Initial NASA Solar Irradiance Science Team (SIST) Program

Key Points:
- The Naval Research Laboratory's solar variability models, NRLTSI2 and NRLSSI2, establish the Solar Irradiance Climate Data Record (CDR)
- The CDR total and spectral (between 265 and 500 nm) solar rotational estimates are validated by observations on 27-day solar rotations
- On solar cycle timescales and longer, particularly in the spectrum, differences in observational data sets preclude model validation

Correspondence to:
O. Coddington,
odele.coddington@lasp.colorado.edu

Citation:
Coddington, O., Lean, J., Pilewskie, P., Snow, M., Richard, E., Kopp, G., et al. (2019). Solar Irradiance variability: comparisons of models and measurements. *Earth and Space Science*, *6*, 2525–2555. https://doi.org/10.1029/2019EA000693

Received 29 APR 2019
Accepted 11 OCT 2019
Accepted article online 08 NOV 2019
Published online 28 DEC 2019

Solar Irradiance Variability: Comparisons of Models and Measurements

O. Coddington[1], J. Lean[1,2], P. Pilewskie[1], M. Snow[1], E. Richard[1], G. Kopp[1], C. Lindholm[1], M. DeLand[3], S. Marchenko[3], M. Haberreiter[4], and T. Baranyi[5,6]

[1]Laboratory for Atmospheric and Space Physics, University of Colorado Boulder, Boulder, CO, USA, [2]Naval Research Laboratory, Washington, DC, USA, [3]Science Systems and Applications, Inc., Lanham, MD, USA, [4]Physikalisch-Meteorologisches Observatorium, Davos, Switzerland, [5]Debrecen Heliophysical Observatory, Debrecen, Hungary, [6]Deceased, 24 July 2018

Abstract The Earth system responds to solar variability on a wide range of timescales. Knowledge of total solar irradiance (TSI) and solar spectral irradiance (SSI) spanning minutes to centuries is needed by scientists studying a broad array of research applications. For these purposes, the NOAA National Centers for Environmental Information (NCEI) Climate Data Record Program established the Solar Irradiance Climate Data Record. Version 2 of the Naval Research Laboratory's solar variability models that are derived from and demonstrate consistency with irradiance observations specifies TSI and SSI for the Solar Irradiance Climate Data Record. We establish the veracity of the Naval Research Laboratory models on the timescales and over the wavelength range for which the Sun is known to vary and, thereby, specify the utility of these models. Through comparisons with irradiance observations and independent models, we validate NRLTSI2 estimates of TSI on solar rotational (~27-day), solar cycle (~11-year), and multidecadal (spacecraft era) variability timescales. Similarly, we validate NRLSSI2 estimates of SSI rotational variability in the ultraviolet through the mid-visible spectrum. Validation of NRLSSI2 estimates at longer wavelengths, particularly in the near-infrared, and for the full spectrum at solar cycle timescales and longer is not possible with the current observational record due to instrumental noise and instrument instability. We identify where key new data sets, such as observations from the Total and Spectral Solar Irradiance Sensor-1, are expected to provide a fuller understanding of total and spectral solar irradiance variability on multiple timescales.

Plain Language Summary An understanding of total and spectral solar irradiance is essential for Earth atmospheric and climate studies because the Sun's energy incident at the top of Earth's atmosphere is the dominant energy source driving a myriad of interactions that establish Earth's climate. We describe how the National Oceanographic and Atmospheric Administration's Solar Irradiance Climate Data Record is meeting the goal to model variability in the Sun's irradiance, identify limitations in our current understanding of solar irradiance variability on multiple timescales and over a broad spectral range, and highlight where new observations are expected to provide a fuller understanding.

1. Introduction

The Sun's power per unit area, or irradiance, dominates other external sources of energy incident for Earth's atmosphere by a factor of almost 4,000 (Kren et al., 2017) and drives a myriad of land, ocean, and atmosphere interactions that define our terrestrial habitat including surface temperature. These interactions are functions of wavelength because the Sun's energy output is spectrally dependent and because the molecules, clouds, and aerosols of Earth's atmosphere and the distinct surface types, such as forest, desert, ocean, etc., scatter and absorb energy in wavelength-dependent ways. Therefore, the total solar irradiance, or TSI (in units of $W{\cdot}m^{-2}$), and the solar spectral irradiance, or SSI (in units of $W{\cdot}m^{-2}{\cdot}nm^{-1}$), provide important upper atmosphere boundary conditions in atmospheric and environmental research that are important for understanding Earth's climate (Stephens et al., 2012). Knowledge of SSI is additionally essential for understanding Earth's atmospheric response to solar energy (Solomon et al., 2007).

The Earth system response to solar variability occurs on a wide range of timescales. As such, a wide variety of community research applications require knowledge of TSI and SSI from minute to century timescales. Examples of these applications include regional and global climate modeling (e.g., Matthes et al., 2017), atmospheric chemistry studies (e.g., Egorova et al., 2004; Swartz et al., 2012), renewable energy research (e.g., Gueymard et al., 2002), and radiative transfer modeling (Clough et al., 1992; Clough et al., 2005) where solar variability based on the NRLSSI2 model has been introduced to the atmospheric Line-By-Line Radiative Transfer Model in conjunction with the new Atmospheric and Environmental Research model (http://rtweb.aer.com/solar_frame.html). To meet the diverse needs of the various research communities, the National Atmospheric and Oceanic Administration's (NOAA) NCEI established the Solar Irradiance Climate Data Record (CDR) in 2015. The irradiances, uncertainties, supporting documentation, and ancillary data for the Solar Irradiance CDR for TSI and for SSI are available at the NOAA websites (https://www.ncdc.noaa.gov/cdr/atmospheric/total-solar-irradiance and https://www.ncdc.noaa.gov/cdr/atmospheric/solar-spectral-irradiance).

Current knowledge of solar irradiance variability is derived primarily from space-based data sets. The observational records of TSI and ultraviolet (UV) SSI are 40 years long, while observations of daily solar irradiance at visible (VIS) wavelengths through the near-infrared up to 2.4 microns span 15 years. This extant solar irradiance database comprises measurements made by individual instruments that differ in their accuracy, stability, and spectral range and resolution, which affects how well the individual records can be combined into a single, longer-term record (Ermolli et al., 2013). For SSI, an additional challenge comes from temporal gaps in the observational record that preclude using measurement overlap from multiple instruments to place individual records on a common calibration scale in a manner that has been very beneficial for developing TSI observational composites (Frohlich, 2006b; Kopp & Lean, 2013; Willson & Mordvinov, 2003). The NASA Solar Radiation and Climate Experiment (SORCE) (Rottman, 2005) achieved important advances in observations of solar irradiance by measuring TSI with the highest accuracy, the lowest noise, and the highest inherent stability to date (Kopp, 2014; Kopp & Lean, 2011) concurrently with the first daily space-based observations of spectrally resolved SSI longward of 400 nm. In addition to its TSI instrument (Kopp & Lawrence, 2005), SORCE measures SSI from X-ray to near-infrared wavelengths with three instruments (Harder et al., 2005; McClintock et al., 2005; Woods & Rottman, 2005).

The SORCE observational advances motivated the development of an updated version (version 2) of the Naval Research Laboratory's (NRL) solar variability models. The updated NRLTSI2 and NRLSSI2 models (Coddington et al., 2016; Coddington & Lean, 2015), respectively, specify total and spectral solar irradiance annually since 1610 and daily since 1882 for the operational NOAA Solar Irradiance CDR. The NRL models estimate irradiance by using relationships between proxy indicators of solar magnetic variability and solar irradiance observations. For the original NRLTSI and NRLSSI models (Lean, 2000; Lean et al., 2005; Lean & Woods, 2010), the observations predated the launch of the SORCE spacecraft. At wavelengths not covered by daily instrumental observations (i.e., longer than 400 nm for the original models and longer than 2400 nm for version 2), the NRL models estimate solar irradiance using theoretical estimates of the contrasts of magnetic features. For time periods prior to the spacecraft-based record, the models estimate solar irradiance using proxy records of solar activity that span long time periods, such as sunspot numbers and cosmogenic isotopes archived in ice cores and tree rings (Lean, 2018). The NRL models have been used in many studies of Earth's climate such as the Coupled Model Intercomparison Project (Matthes et al., 2017) and the Paleoclimate Model Intercomparison Project (PMIP) (Schmidt et al., 2011) and in review assessments of Earth's climate by the Intergovernmental Panel on Climate Change (Schimel, 1996; Shine et al., 1990; Solomon et al., 2007).

There are other published solar irradiance variability models that have a similarly broad wavelength coverage and long time span needed for climate model studies. These models are similar to the NRL models in that they assume that magnetic variability on the Sun drives irradiance variability, but they extract their magnetic-to-irradiance variability relationship in different ways. For example, the Spectral and Total Irradiance Reconstructions for the Satellite Era (SATIRE-S) model (Yeo et al., 2014) derives the magnetic-to-irradiance variability relationship using a physical, theoretical model of the solar atmosphere that specifies the contrast of magnetic features relative to a feature-free quiet Sun, with irradiance variability then being based on images of magnetic activity on the Sun (i.e., magnetograms). Prior to the spacecraft era, the SATIRE-T model (Krivova et al., 2010) extracts its inputs from proxies of solar activity and a model to estimate the historical time evolution of magnetic activity. The Empirical Irradiance Reconstruction (EMPIRE) model (Yeo, Krivova, et al., 2017), like the NRL models, computes coefficients that scale proxies of magnetic activity into irradiance change but uses a different underlying statistical regression methodology than NRL. EMPIRE extends back only to 1947. For all models, confidence in estimates of past solar irradiance as well as model predictions at wavelengths beyond the currently observed ranges is gained by demonstrating consistency with the observations.

Measurements and models of solar irradiance variability are now sufficiently mature to enable the NOAA NCEI Climate Data Record Program to provide the science community with a solar irradiance climate data record of sufficient length, consistency, and continuity to determine climate variability and change (NRC, 2004). The NOAA Solar Irradiance CDR falls under the *thematic* climate data record designation as a "blend of satellite observations, in-situ data, and/or model output." The NOAA Solar Irradiance CDR extends prior to the spacecraft era, providing understanding of solar variability at much longer timescales and over a broader range in wavelengths than possible from the observational record alone.

Uncertainty remains, however, in understanding the wavelength dependence of solar irradiance variability and the magnitude of multidecadal changes. The National Aeronautics and Space Administration (NASA) established a Solar Irradiance Science Team (SIST) based on a 2014 ROSES solicitation with the aim of providing to the Earth science community the most reliable specification of solar irradiance that includes consistent multi-instrument and multiplatform spacecraft records of solar irradiance. The expected outcomes of these initial SIST efforts include improved observational irradiance records that have superior utility as input to global models such that the effects of variations in solar output and subsequent impacts on the Earth system are better represented. For example, the competitively selected SIST teams are reprocessing and recalibrating SSI observations from the Ozone Monitoring Instrument (OMI) (Marchenko et al., 2019), the Solar Mesosphere Explorer, the Active Cavity Radiometer Irradiance Monitor (ACRIM), and the SORCE mission, including developing an alternative approach for correcting SORCE SIM degradation (Mauceri et al., 2018); improving and extending an existing SSI composite (DeLand et al., 2019); developing a SORCE SSI record for chemistry-climate studies (Harder et al., 2019); developing a new TSI observational composite using modern composite methodology approaches; improving observational composites of Lyman-alpha irradiance (Machol et al., 2019) and the magnesium (Mg) II index; and developing new versions of the NRL solar variability models (i.e., NRLTSI3 and NRLSSI3) that incorporates knowledge gained from these activities.

The purpose of this paper is to compare version 2 of the NRL modeled irradiances to TSI and SSI observations and observational composites as well as to independent models of solar irradiance variability. Since the implementation of the NOAA Solar Irradiance CDR, solar irradiance observations have lengthened, new observations and observational composites have been produced, and new irradiance variability models have been developed. We aim to validate the performance of the models transitioned to the NOAA Solar Irradiance CDR, quantify current understanding about solar irradiance variability, and identify areas where differences across data sets demonstrate that a fuller understanding of solar irradiance variability remains incomplete. In particular, whenever possible, we identify prospects for new understanding and future improvements in the NRL models using state-of-the-art observations now being made by NASA's Total and Spectral Solar Irradiance Sensor-1 (TSIS-1), launched to the International Space Station in late 2017.

Section 2 of this paper describes the NRLTSI2 and NRLSSI2 model formulation, uncertainty estimation, and transition to the NOAA CDR operational program, including ongoing stewardship. Section 3 compares the NRLTSI2 model with multiple observations and independent models of variability on timescales of the solar rotational period and solar cycle during the spacecraft era. Section 4 is analogous to Section 3 but addresses the NRLSSI2 model of SSI variability. In Section 5, we discuss the results and identify the approaches for extending the NOAA Solar Irradiance CDR in time and for incorporating new and improved data sets as model inputs and as quality assurance of the CDR irradiance estimates. Summary statements follow in Section 6.

2. The NRLTSI2 and NRLSSI2 Solar Irradiance Variability Models

The NRLTSI2 and NRLSSI2 solar variability models determine the changes in solar irradiance from specified background quiet Sun conditions that occur with changes in solar magnetic activity. Bright faculae and dark sunspots are visible manifestations of this magnetic activity on the Sun's surface (i.e., the lowermost layer of the Sun's atmosphere called the photosphere). By using a multiple linear regression analysis of proxy indices of the Sun's magnetic activity with observations of TSI and SSI, the modeled irradiances are computed by relating incremental changes in the observed proxy activity into an equivalent irradiance change.

2.1. Model Formulation

Here we provide an overview of the algorithm that calculates the $TSI(t)$ and $SSI(\lambda,t)$, at a specified time, t, and wavelength, λ. The algorithm assumes that when faculae and sunspots are present on the solar disk, the facular brightening, $F(t)$, and sunspot darkening, $S(t)$, alter an assumed, static, baseline solar irradiance (quiet Sun) that corresponds to the irradiance in their absence. The time dependence in the modeled irradiances comes from indices for facular brightening and sunspot darkening at a specified time. Coddington and Lean (2015) and Coddington et al. (2016) provide full algorithm details.

For $TSI(t)$, the irradiance is altered from quiet Sun TSI, TSI_Q, by amounts $\Delta TSI_F(t)$ and $\Delta TSI_S(t)$, respectively, so that

$$\mathrm{TSI(t)} = \mathrm{TSI_Q} \quad + \Delta\mathrm{TSI_F(t)} + \Delta\mathrm{TSI_S(t)}.$$

Similarly the faculae and sunspots alter the spectral irradiance from specified baseline, $SSI_Q(\lambda)$, by wavelength-dependent amounts, $\Delta SSI_F(\lambda, t)$ and $\Delta SSI_S(\lambda, t)$, so that

$$\mathrm{SSI}(\lambda, \mathrm{t}) = \mathrm{SSI_Q}(\lambda) + \Delta\mathrm{SSI_F}(\lambda, \mathrm{t}) + \Delta\mathrm{SSI_S}(\lambda, \mathrm{t}).$$

The integral of the spectral irradiance equals the corresponding total irradiance at any time, t, and for the static quiet Sun:

$$\mathrm{TSI(t)} = \int_{\lambda_0}^{\lambda_\infty} \mathrm{SSI}(\lambda, \mathrm{t})\mathrm{d}\lambda,$$

$$\mathrm{TSI_Q} = \int_{\lambda_0}^{\lambda_\infty} \mathrm{SSI_Q}(\lambda)\mathrm{d}\lambda,$$

Time-dependent values for the facular brightening, $F(t)$, and sunspot darkening, $S(t)$, that are derived from proxy indices of magnetic variability produce incremental changes in TSI:

$$\Delta\mathrm{TSI_F(t)} \propto \mathrm{F(t)},$$

$$\Delta\mathrm{TSI_S(t)} \propto \mathrm{S(t)},$$

and in SSI:

$$\Delta\mathrm{SSI_F}(\lambda, \mathrm{t}) \propto \mathrm{F(t)},$$

$$\Delta\mathrm{SSI_S}(\lambda, \mathrm{t}) \propto \mathrm{S(t)},$$

and are constrained such that the integral of the facular and sunspot contribution to the spectral irradiance equals the corresponding contribution to the total irradiance:

$$\Delta\mathrm{TSI_F(t)} = \int_{\lambda_0}^{\lambda_\infty} \Delta\mathrm{SSI_F}(\lambda, \mathrm{t})\mathrm{d}\lambda,$$

$$\Delta\mathrm{TSI_s(t)} = \int_{\lambda_0}^{\lambda_\infty} \Delta\mathrm{SSI_S}(\lambda, \mathrm{t})\mathrm{d}\lambda.$$

The specified baseline quiet Sun solar irradiance is based on SORCE observations during a time when solar activity was minimal (Woods et al., 2009). The SSI observations, spanning 115 to 2400 nm, are augmented between 300 and 1000 nm by SOLar SPECtrum (SOLSPEC) observations on the ATLAS mission (Thuillier et al., 1998). Above 2400 nm, the Kurucz (1991) theoretical spectrum is used. A normalization of the integral of the quiet Sun reference spectrum constrains its value to 1360.45 W/m^2, the quiet Sun TSI consistent with the 2008 solar minimum SORCE TSI value of 1360.8 $\pm$0.5 W/m^2 (Kopp & Lean, 2011).

SORCE TSI and SSI observations between the years 2003 and 2014 are used to derive the regression coefficients that scale changes in proxy indices of facular brightening and sunspot darkening from their specified quiet Sun values to irradiance change. Specifically, observations of TSI are from the Total Irradiance Monitor (TIM) (Kopp et al., 2005) and observations of SSI from the SOLar STellar Irradiance Comparison Experiment (SOLSTICE) (McClintock et al., 2005) and Spectral Irradiance Monitor (SIM) (Harder et al., 2005). The irradiance changes then increase or decrease the specified baseline irradiance, depending on the net effect of the strengths of the facular and sunspot influences at any time. The time-invariant scaling coefficients describing the offset and slope of the linear relationship between irradiance observations and the proxy indices are scalar values for NRLTSI2 and functions of wavelength for NRLSSI2 (Coddington et al., 2016; Coddington & Lean, 2015). Therefore, the time-dependent variability in the modeled irradiances comes from the time dependence in the proxies themselves due to solar rotation and overall activity variations (emergence, evolution, and disappearance of active regions) throughout the approximately 11-year solar cycle.

The coefficients of the NRLTSI2 model are derived using regressions between TIM observations and proxies with no additional corrections applied. However, to quantitatively reproduce spectral irradiance observations throughout the solar cycle, corrections are applied to the initial coefficients of NRLSSI2, the spectral irradiance variability model, which are derived over the shorter timescales of solar rotation. This is because the SORCE SSI observations have poorer long-term stability than the SORCE TSI observations (Lean & DeLand, 2012). Moreover, the proxy indices of facular brightening and sunspot darkening are imperfect indicators of faculae and sunspots that have observational error. Therefore, corrections scale the SSI-model regression coefficients derived from irradiance observations at solar rotation timescales to solar cycle timescales and ensure that the integral of the facular and sunspot contribution to the spectral irradiance equals the corresponding contribution to the total irradiance. The corrections are determined by the TSI variability and implemented for the separate facular and sunspot proxy records such that the integral of the SSI change due to facular and sunspot activity equals their respective contributions to the TSI (Coddington & Lean, 2015). While the magnitude of this correction is modest compared with the assumed uncertainty in the proxy indices themselves, it adds a small additional uncertainty to the modeled irradiances.

An additional component to the modeled facular index when reconstructing irradiance change prior to approximately 1950 addresses the speculation that faculae cause longer-term irradiance changes over decades to centuries from an accumulation of magnetic flux that underlies the solar cycle. In the NRLTSI2 and NRLSSI2 models, a magnetic flux transport model was used to simulate the eruption, transport, and accumulation of magnetic flux on the Sun's surface, after which the resulting net increase in facular brightness is added to the modeled irradiances as a background term (Wang et al., 2005).

The new NRLTSI3 and NRLSSI3 models also use multiple linear regression parameterizations of facular brightening and sunspot darkening proxy indices and SORCE TSI and SSI irradiance observations to relate incremental change in the proxy inputs to equivalent irradiance change. However, the NRLTSI3 and NRLSSI3 models differ from the version 2 NRL models because they specify the facular brightening influence as a combination of linear and exponential terms. Additionally, the new models adopt an alternative sunspot darkening index derived from the Debrecen, Hungary, catalog of observations. Both of these changes were found to provide statistically significant improvements in model performance.

2.2. Model Inputs

With the NRLTSI2 and NRLSSI2 model coefficients established from multiple linear regression against SORCE observations, the models calculate solar irradiance at any given time given two inputs; a facular index and a sunspot index.

Disk-integrated irradiance observations of the magnesium (Mg) II index compiled into a composite record by the University of Bremen are the adopted proxy for facular brightening (Snow et al., 2014). The University of Bremen's composite Mg II index record is available from its website (http://www.iup.uni-bremen.de/gome/gomemgii.html). The Mg II index is a disk-integrated ratio of irradiance measurements from the core of the Mg II emission line at 280 nm that varies with chromospheric activity to irradiance measurements from the nearby wings of the emission line (at 278 and 282 nm) where variability originates in the much quieter photospheric layer of the Sun (Snow, McClintock, Rottman, & Woods, 2005; Snow, McClintock, Woods, et al., 2005; Viereck et al., 2001). As such, it is a sensitive indicator of magnetically enhanced bright regions and has been measured from space since 1978. By choosing the Mg II index as the proxy of facular brightening, we assume that the chromospheric activity, which dominates the core emissions, is an extension of the underlying faculae in the photospheric layer of the Sun. While the nature of ratio measurements of irradiances taken in nearby wavelengths potentially makes the Mg II index independent of instrumental sensitivity changes, the time series of Mg II index from different instruments and from different spacecraft platforms do not always exhibit identical temporal behavior even after correcting for spectral resolution differences. Uncorrected instrumental artifacts are a potential source of this behavior (Snow et al., 2014).

The proxy of sunspot darkening is derived from direct, daily observations of the number of sunspots and areas on white-light images of the solar disk by ground-based observatories; the heliocentric locations are used to account for variations in sunspot contrast as a function of limb position (e.g., Lean et al. (1998)). For the Solar Irradiance CDR, the sunspot darkening is derived from an unweighted average from a network of ten stations in the U.S. Air Force Solar Observing Optical Network (SOON), which has been making daily observations since 1976. The USAF/SOON sunspot information is archived by NCEI; formerly the National Geophysical Data Center. The data are available at the website www.ngdc.noaa.gov/stp/spaceweather.html. From 1882 to 1976, these sunspot observations were made by the Royal Greenwich Observatory (RGO). In v02r00 (i.e., the original release of the NRL2 family of modeled irradiances), we reduced RGO areas by 25% to correct for a systematic difference from the SOON scale (Fligge & Solanki, 1997). However, in v02r01, we adopt a 45% reduction in RGO areas (Hathaway, 2010), a change that has been supported by a correlation analysis with an independent sunspot number record. Prior to 1976, v02r00 and v02r01 irradiance estimates differ, with maximum differences in daily TSI of approximately 1 W/m^2.

From 1940 to 1978, the proxy for facular brightening is a composite record of chromospheric activity constructed by Lean et al. (2001) that utilizes space- and ground-based observations of additional indicators of chromospheric activity. From 1882 to 1940, the facular brightening composite record is derived through cross correlating the ground- and space-based direct observations of chromospheric activity with the daily group sunspot number record (Hoyt & Schatten, 1998).

Prior to 1882, the only available record of solar activity is the group sunspot number, which precludes the use of independent facular and sunspot inputs to the model. For this reason, irradiance estimates prior to 1882 are provided only as yearly values determined by the relationship of the annually averaged modeled irradiance after 1882 (i.e., the net change of the facular and sunspot influences) with annual sunspot numbers. Extension of the NRLTSI2 and NRLSSI2 irradiance estimates from 1610 to 850 CE uses the correlation of average of irradiance variations modeled using two different sunspot number records with cosmogenic isotopes (Lean, 2018).

2.3. Uncertainty Estimates

Accompanying the NRLTSI2 and NRLSSI2 modeled irradiances are uncertainties that are derived from uncertainties in the facular brightening and sunspot darkening values (specified as ±20% relative change from their values at solar minimum) propagated into irradiance units combined with statistical fitting uncertainties of the scaling coefficients (Coddington et al., 2016; Coddington & Lean, 2015). These uncertainties reflect the uncertainty in the modeled irradiances at any given time relative to solar minimum conditions and are a function of time and, for SSI, also of wavelength. For v02r00, the uncertainties for the delivered NRLSSI2 data were provided in separate files because file size limitations precluded their inclusion in the same file as the irradiances. However, for v02r01, these limitations were overcome, and the delivered NRLSSI2 data files contain the irradiance estimates and their associated uncertainties. There is an additional component to the NRLTSI2 and NRLSSI2 uncertainties that is not reflected in the delivered data and that comes from the absolute accuracies of the instruments used in measuring the reference quiet Sun TSI and SSI (Kopp & Lean, 2011; Woods et al., 2009). Tables 5 and 7 in Coddington and Lean (2015) provide examples of estimating a total uncertainty for NRLTSI2 and NRLSSI2 that combines the statistical and systematic uncertainties.

2.4. Quality Assurance

The Solar Irradiance CDR is an operational product. As such, we enact quality assurance to ensure the fidelity of the modeled irradiances that we submit regularly to NOAA to extend the CDR from 2015 to the present. The modeled irradiances are sensitive to the proxy indices chosen to represent the true solar variability, so the stability of the modeled irradiances depends in part upon the stability of the model inputs. We verify the proxy inputs through a suite of numerical tests that include automatic and manual diagnostics, flagging of anomalous values, calculations of deviations from expected or predicted values, and trending of the facular brightening and sunspot darkening indices relative to independent proxies of solar variability (see below). These verifications are regularly performed quarterly and annually with the goal of identifying spurious values and changes in long-term trends between the proxy variables used in the model and the independent proxies against which the model inputs are evaluated. To facilitate independent analysis of our model inputs, we make the model input indices publicly available as part of the ancillary data delivery for the Solar Irradiance CDR.

Currently, quality assurance for the operational NOAA Solar Irradiance CDR involves monitoring the accuracy and long-term stability of the University of Bremen's Mg II index facular brightening function through statistical correlations with seven independent sources of proxies of solar chromospheric variability. These include the Mg II and Ca II indices from the OMI on the AURA spacecraft (DeLand & Marchenko, 2013), the Ca K index from the National Solar Observatory's Sacramento Peak Observatory (Keil et al., 1998) and the California State University, Northridge San Fernando Observatory (Chapman et al., 1997; Steinegger et al., 1996), and the F10.7-cm radio flux observed by the Solar Radio Monitoring Program at the Dominion Radio Astrophysical Observatory (Tapping, 2013). In the future, we plan to incorporate the NASA's SIST Mg II observational composite in our model assessment and QA analysis. We monitor the accuracy and long-term stability of the SOON network sunspot blocking function through statistical correlations with independent records of sunspot darkening. Independent sources of sunspot area measurements include the Active Region Database of USAF/SOON data (Hathaway et al., 2002), the San Fernando Observatory (Chapman et al., 1997), and the Debrecen Heliophysical Observatory in Debrecen, Hungary (Gyori et al., 2011).

The QA for the Solar Irradiance CDR also monitors internal consistency in the models by comparing the spectrally integrated SSI with the TSI, including the separate facular brightening and sunspot darkening components. For successive time periods (i.e., 1978 to 2014, 1978 to 2015, etc. through present day), we monitor statistical metrics of the integrated modeled SSI and the independently modeled TSI and the integrated spectral facular brightening and sunspot darkening with their bolometric equivalents. Thus far, these metrics are essentially unchanged from those published with the original release of the NRL2 family of models (Coddington et al., 2016). An additional important component of the QA for the Solar Irradiance CDR is validation of the modeled irradiances by comparisons with observations and with other models. Such comparisons, the motivation behind this paper, are presented in Sections 3 and 4.

2.5. Operational Implementation

The Laboratory for Atmospheric and Space Physics (LASP) at the University of Colorado Boulder is responsible for the operations and data delivery of the Solar Irradiance CDR. Preliminary irradiance values, associated uncertainties, and ancillary data are delivered to the NCEI every quarter, following initial delivery in 2015. After completion of the quality assurance, the preliminary data are replaced with final data on an annual basis. CDR production at LASP utilizes the LaTiS software framework that provides a web service interface between the model inputs and the processing code, as a part of the LASP Interactive Solar Irradiance Datacenter (Hunter et al., 2018).

Bates et al. (2016) describe the requirements for adopting a record as a NOAA CDR, a process that begins with an assessment of the readiness of a candidate data record to *transition* from research to operations. The readiness to transition in six key areas is quantified in a maturity matrix (Bates & Privette, 2012). The NRL solar variability models were transitioned to the NOAA's NCEI in Asheville, NC, as the Solar Irradiance CDR in 2015. The NRL models, having been described in multiple peer-reviewed journal articles and adopted for widespread use in the science community, further established their readiness for transition after a systematic and reproducible data generation mechanism was demonstrated and after supporting documentation including source code, an algorithm theoretical basis document, and associated ancillary data were complete and made publicly available. The NOAA CDR program has a revision process to incorporate and document research advances to ensure consistent and continuous data production over many decades (i.e., traceability). The initial version of the Solar Irradiance CDR was designated "version 2" (v02r00) to distinguish it from earlier manifestations of the NRL models that had different scaling coefficients because they were derived from pre-SORCE era irradiance observations and activity indices. The first revision (v02r01) of the Solar Irradiance CDR, published in 2017, incorporated new sunspot number research that impacted the time series of model inputs. We anticipate a version update of the Solar Irradiance CDR in another 1 to 2 years that incorporates the advancements of the version 3 NRL models and that incorporates observations from TSIS-1. NCEI maintains the NOAA CDR records including the preservation of all published versions and revisions.

A collection of ancillary data and documentation is delivered with the Solar Irradiance CDR. These include 1-nm resolution modeled reference spectra for varying levels of solar activity and during the Maunder minimum period (around the year 1650) when the Sun was devoid of solar activity cycles as identified by a lack of spots in recorded sunspot number records. Also provided is the 1-nm resolution, measurement-based, quiet Sun reference spectrum. For v02r01, two records of modeled pre-1882 annually averaged irradiances are provided based on different versions of the daily sunspot number record (Clette et al., 2014; Clette et al., 2015; Hoyt & Schatten, 1998). Additionally, an observational TSI composite is delivered. In v02r01, this composite is defined as the average of three individual composite records that are separately normalized to the SORCE TIM absolute scale. The individual records are the ACRIM composite (Willson & Mordvinov, 2003), the Physikalisch-Meteorologisches Observatorium Davos (PMOD) composite (Frohlich & Lean, 1998), and the Royal Meteorological Institute of Belgium (RMIB) composite (Dewitte & Nevens, 2016). These composite data sets contribute to the Solar Irradiance CDR observational TSI composite prior to the SORCE era after which time the CDR observational TSI composite is extended with the direct SORCE TIM TSI observations. In future versions, we expect to incorporate the direct TSIS observations and may replace the CDR TSI observational composite with a new observational composite developed under NASA's SIST program.

3. Comparisons of TSI Variability Models and Measurements

We compare the NRLTSI2 model to observations, observational composites, and independent models of solar variability with the goal of ensuring the fidelity of the NOAA Solar Irradiance CDR in addition to providing further quality assurance of the input indices (Section 2.4). The comparisons are made on different timescales for which the Sun is known to vary: the 27-day solar rotational cycle (Section 3.1) and the 11-year solar activity cycle (Section 3.2).

We employ a number of independent data sets in our TSI comparisons, including direct observations made by TIM on SORCE (Kopp et al., 2005) and the TSI Calibration Transfer Experiment (TCTE) (Kopp, 2014), the ACRIM, PMOD, and RMIB composites and a preliminary version of a new composite developed as part of SIST called the Community-Consensus TSI composite. We also include the SATIRE-S model (Yeo et al., 2014), the EMPIRE model (Yeo, Krivova, et al., 2017), a three-dimensional extension of the SATIRE-S model (SATIRE-3D) (Yeo et al., 2017), and a new NRL model version, NRLTSI3.

Version 17, level 3 SORCE TIM data were sourced from the SORCE website (http://lasp.colorado.edu/home/sorce/data/). The ACRIM composite, version 20131130, is available from http://www.acrim.com/Data_Products.htm website. The PMOD composite is available from ftp://ftp.pmodwrc.ch/pub//data/irradiance/composite/DataPlots/composite_42_65_1709.dat website. The RMIB composite, version 20161010, is available from ftp://gerb.oma.be/steven/RMIB_TSI_composite/RMIB_TSI_composite_latest.txt website. The preliminary Community-Consensus TSI composite, v0.1, is available from Greg Kopp. SATIRE-S (version date 20180329), EMPIRE (version date 20170531) and SATIRE-3D (version date 20160731) data were all sourced from http://www2.mps.mpg.de/projects/sun-climate/data.html.

3.1. TSI on Solar Rotational Timescales

The rotation of the Sun on its axis alters the population of faculae and sunspots projected toward Earth, producing an approximate 27-day irradiance modulation. To isolate model-to-measurement comparisons on this timescale, we detrend each data set by removing an 81-day running mean; the resultant time series

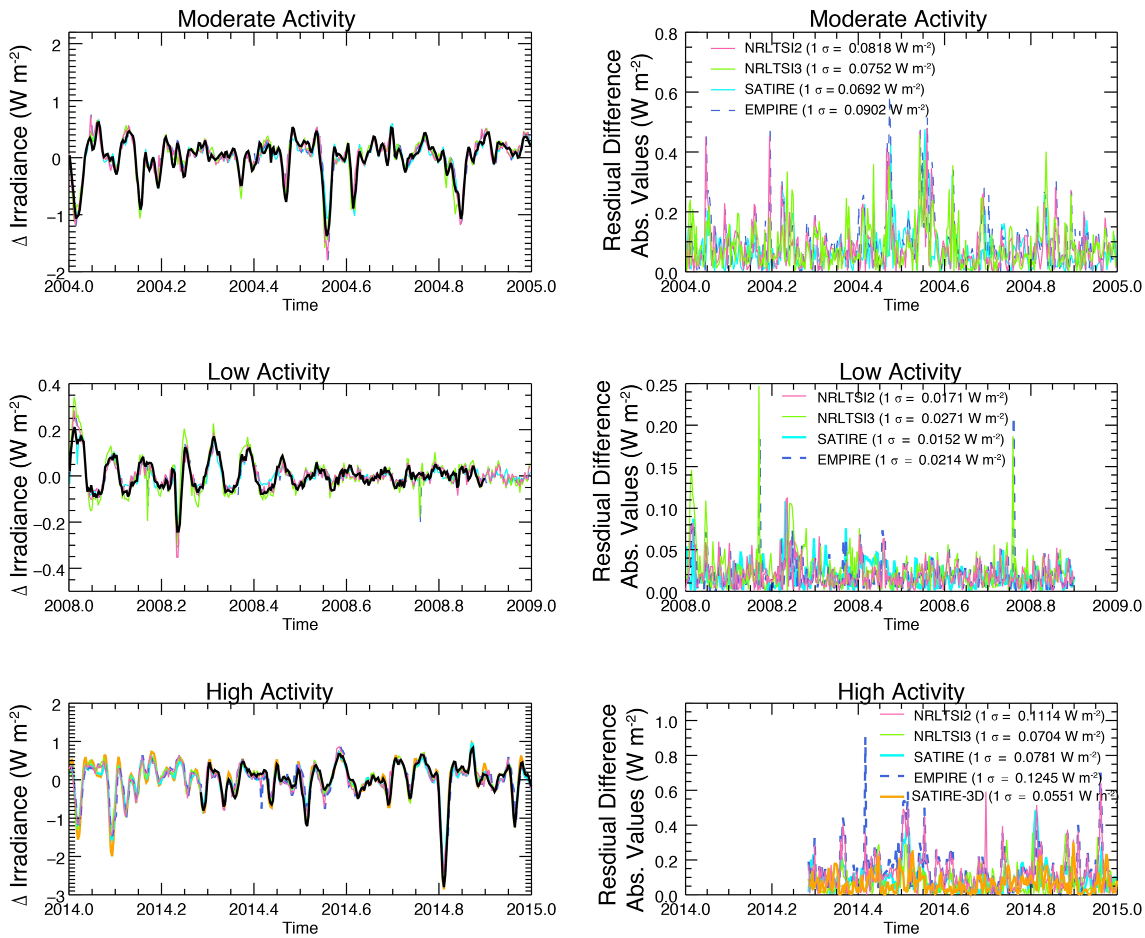

Figure 1. Times series of rotational TSI variability (left) and the absolute value of the measurement minus model residual differences (right) for the years 2004 (moderate levels of solar activity), 2008 (low activity), and 2014 (high solar activity). Rotational variability is derived by detrending each time series separately (i.e., removal of an 81-day running mean). The legend provides the 1-sigma standard deviation of the residual differences over each time period.

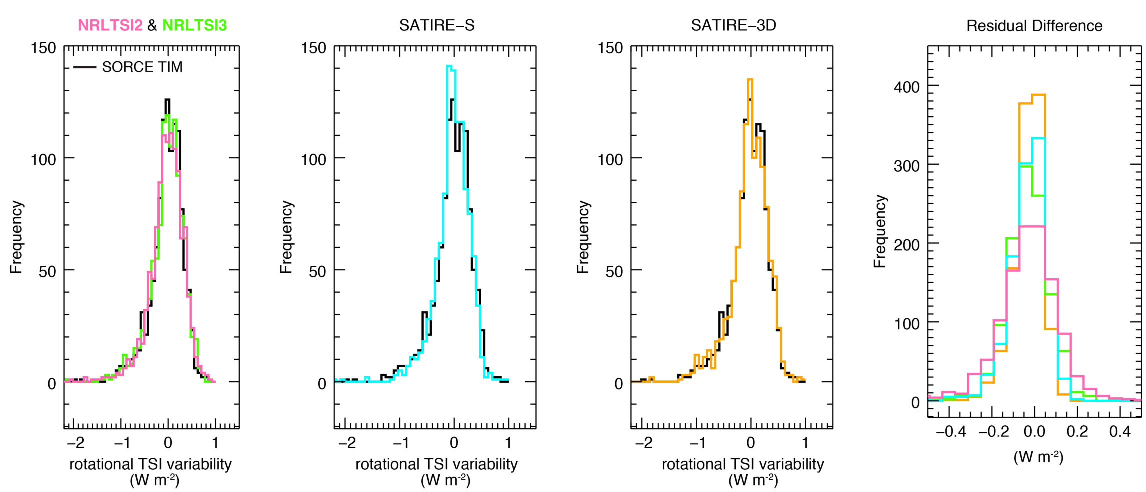

Figure 2. Histograms of rotational TSI variability for the NRLTSI2, NRLTSI3, SATIRE-S, and SATIRE-3D models and the SORCE TIM observations (black). The far-right plot is the histogram of the residual difference (measurement *minus* model) of the rotational TSI variability. The analysis is performed over 1125 days in common among the data sets for the time period 2011 through 2015.

10.1029/2019EA000693

oscillates around zero, free of low frequency trends. Figure 1 shows time series of rotational TSI variability and residual differences for the various models with respect to the SORCE TIM observations (in black) for separate periods of low, moderate, and high solar activity. Dips in the time series are reductions in the TSI due to sunspots, and the irradiance enhancements are due to faculae. In general, the models reproduce observed rotational variability at all levels of solar activity with a mean residual difference better than 0.5 W/m^2 and a 1-sigma standard deviation of the residual difference of 0.1 W/m^2. The SATIRE-3D model, available for the years 2010 to 2016, reproduces rotational TSI variability with a mean residual better than 0.3 W/m^2 during the high-activity period selected here. During the low- and moderate-activity periods, the SATIRE-S model reproduces rotational TSI variability better than the NRLTSI2 and NRLTSI3 models. The EMPIRE model shows the poorest reproduction of rotational TSI variability at moderate- and high-activity solar activity levels.

We extend our statistical investigation of rotational TSI variability to the time period 2011–2015 that encompasses the rising phase of solar activity in cycle 24 and includes the SATIRE-3D model, which spans a shorter time period than the other models. Histograms of rotational variability for the NRLTSI2, NRLTSI3, SATIRE-S, and SATIRE-3D models are compared to SORCE TIM observations in Figure 2 using a common time period for all; also shown are the histograms of the residual differences in the modeled rotational variability relative to the measurements. Results for the EMPIRE model are not shown because they have the same general distribution as NRLTSI2 with only slightly larger residual differences.

All models generally reproduce the distribution of rotational variability in the observed TSI. We find that the NRLTSI3 and SATIRE-3D models perform best in estimating the variability in the TSI observations, particularly for small, near-zero rotational variability, while the NRLTSI2 model generally underpredicts, and the SATIRE-S model slightly overpredicts the small, near-zero rotational variability. The distribution of measurement-minus-model residual difference for the NRLTSI2 and NRLTSI3 models is Gaussian in shape suggesting that these models are balancing over- and underestimations of rotational TSI variability. The histogram of the residual difference for the SATIRE-3D model is the narrowest of all the models and slightly skewed to negative values, reflecting SATIRE-3D's strong overall reproduction of rotational TSI variability while also potentially indicating a small systematic overestimation of rotational variability.

When examining the complete time period of the SORCE TIM record from 2003 through 2017, we continue to find that the SATIRE-S model is marginally better than the NRLTSI2 model at reproducing observed TSI variability. The 1-sigma standard deviation of the residual difference of rotational variability for 4354 days between 2003 and 2017 common between the two models is 0.28 W/m^2 for the SATIRE-S compared to 0.30 W/m^2 for NRLTSI2.

3.2. TSI on Solar Cycle Timescales

The occurrence and areas of sunspots and faculae on the Sun vary during the Sun's 11-year activity cycle, producing an approximate 0.1% increase in solar irradiance during cycle maxima when sunspots and faculae are present in greater numbers. To compare models and measurement on this longer timescale, we smooth each data set time series with an 81-day running mean to remove higher frequency variability. Figure 3 shows the smoothed TSI time series for the SORCE TIM and PMOD observations and the models and the residual differences for the various data sets with respect to SORCE TIM. The SATIRE-3D model spans a subset of the time period from 2010 through 2016.

Table 1 lists the statistical means and standard deviations of the residual differences for the various models with respect to SORCE TIM, computed over days in common among the data sets between 2010 and 2016. Over that time period, the SATIRE-3D model best reproduces SORCE TIM TSI (to zero mean difference and 0.05 W/m^2 standard deviation) followed by NRLTSI2, which has largely similar performance to NRLTSI3 and EMPIRE. The PMOD and SATIRE-S data sets show a different long-term temporal behavior (i.e., a secular trend) than the SORCE TIM observations and the NRLTSI2, NRLTSI3, and EMPIRE models. At the start of the SORCE era, both PMOD and SATIRE-S exceed SORCE TIM TSI while they fall below at the end of the SORCE era. Figure 3 also shows evidence of a growing bias between SORCE TIM observations and NRLTSI2, NRLTSI3, and EMPIRE estimates beginning in 2016.

10.1029/2019EA000693

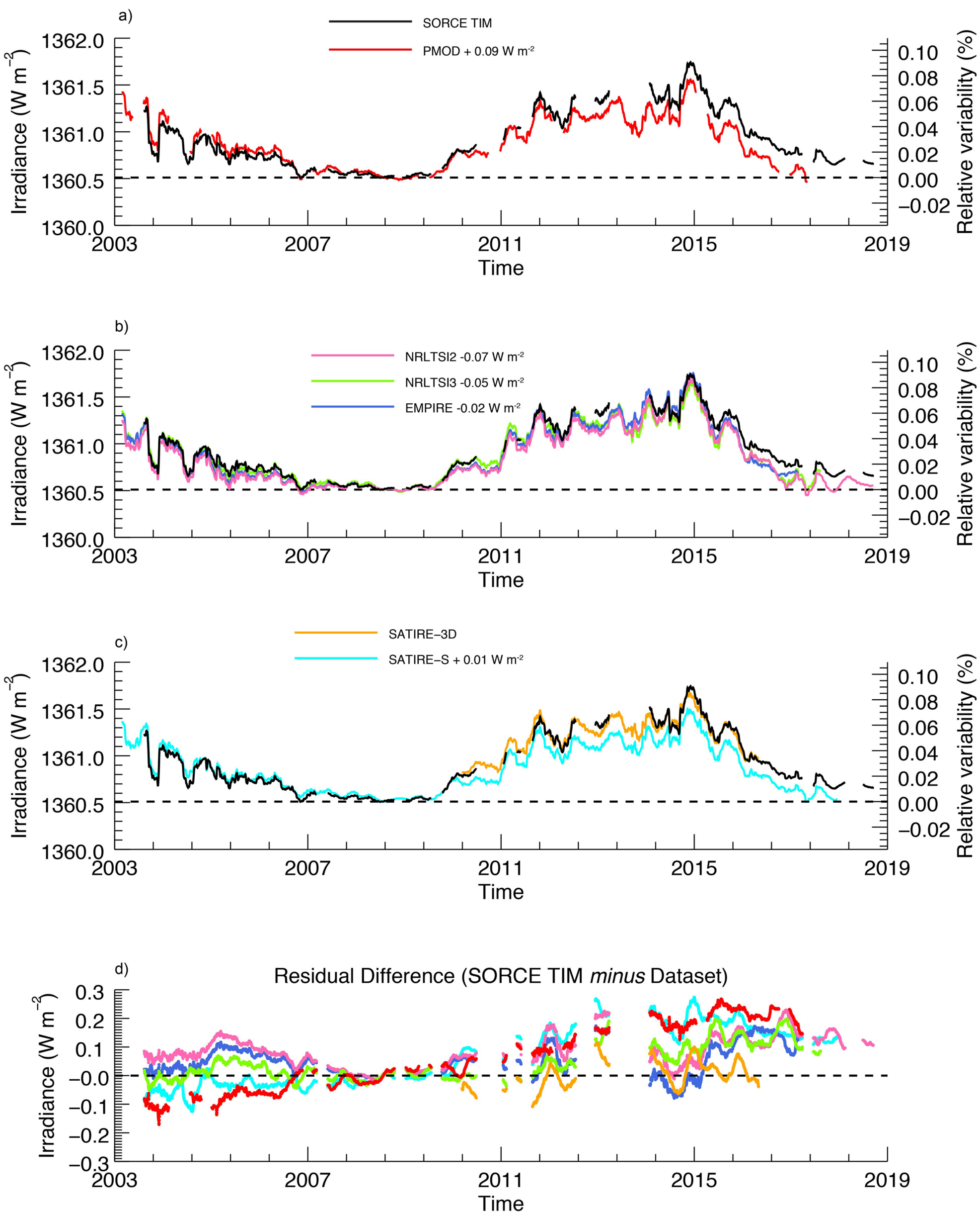

Figure 3. (a–c) TSI solar cycle time series comparison for the SORCE TIM observations (black), PMOD composite, and the models. Each data set has been separately smoothed with an 81-day running mean. Due to differences in absolute scale, data sets have been normalized to the SORCE TIM TSI value during solar minimum conditions (defined as the average of an 81-day period centered on 1 September 2008) as noted in the legend; no scaling has been applied to the SATIRE-3D record. The right-hand y axis is the relative TSI variability (in %) with respect to the solar minimum reference period. (d) The residual difference with respect to SORCE TIM for the various data sets.

Table 1
Mean and 1-Sigma Standard Deviation of the Residual Difference of the Various Data Sets Shown in Figure 3 With Respect to SORCE TIM Computed for 1274 Days in Common Among the Data Sets Between 2010 and 2016

Data set	Mean [W/m^2]	Std. Dev. [W/m^2]
PMOD	0.25	0.06
NRLTSI2	0.03	0.06
NRLTSI3	0.04	0.06
EMPIRE	0.03	0.07
SATIRE-S	0.18	0.05
SATIRE-3D	0.00	0.05

The growing bias between the SORCE TIM measurements and model estimates could be evidence of deficiency in the models to reproduce the observed TSI record, an issue in the SORCE TIM observational record, or some combination of both. Partial time series comparisons of the SORCE TIM TSI observational record with independent observations from the PMOD composite and the TCTE TIM instrument are shown in Figure 4. For approximately 1 year from mid-2015 to mid-2016, the SORCE and TCTE TIM records diverge from each other with discrepancies approaching 0.13 W/m^2, which exceeds their estimated stability of 10 parts per

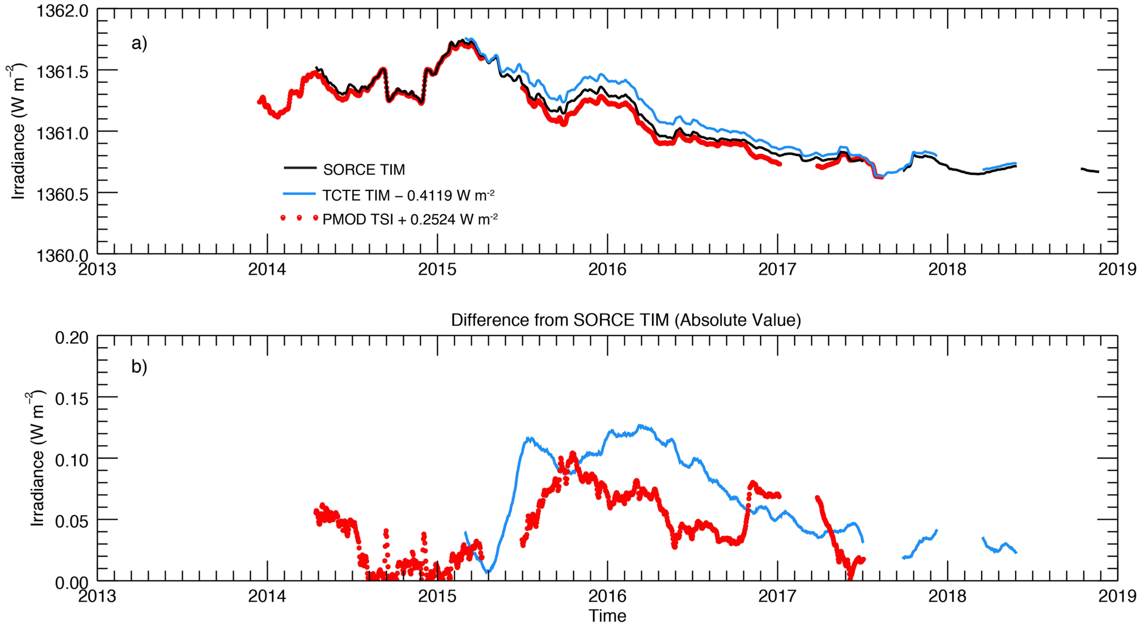

Figure 4. (a) TSI time series for the SORCE TIM and TCTE TIM observations and the PMOD composite records since 2014. The TCTE TIM and PMOD composite have been normalized to the SORCE TIM absolute scale over an 81-day period centered on 13 March 2015; normalization values are identified in the legend. (b) The absolute value of the difference in the TCTE TIM and PMOD TSI records with respect to SORCE TIM.

million (ppm) per year and also exceeds the discrepancy between the PMOD and SORCE TIM instrument records over the same period.

To numerically quantify solar cycle variability, Table 2 provides values of TSI energy change (i.e., irradiance at solar maximum minus the irradiance at solar minimum) for three separate periods during the SORCE era for the SORCE TIM observations and for the PMOD, ACRIM, and RMIB TSI composites and the NRLTSI2, NRLTSI3, EMPIRE, and SATIRE-S models. Although the TSI observations and models differ from each other in non-systematic ways, we infer the following general statements about the ability of the models to reproduce TSI solar cycle energy change, using the SORCE TIM observations as our observational baseline. Of the models, different ones best reproduce TSI energy change in the SORCE TIM observations at different parts of the SORCE record. The largest disagreements in energy change values between the models and the SORCE TIM observations are 8–28%. All the models generally reproduce the energy change in the SORCE TIM observations to a higher degree than most of the TSI composite records. For example, disagreement between the PMOD composite and SORCE TIM observations reaches values of 20%, increasing to 28% for the RMIB composite, and 31% for the ACRIM composite.

Comparing models and observations is more ambiguous over the entire 40-year record of TSI observations. Composite records differ due to their different construction approaches and selected observational subsets and whether or not they incorporate postprocessing corrections to the original data sets from early radiometers (Frohlich, 2006a) that affect the TSI record prior to approximately 1995 (Dudok de Wit et al., 2017). In Figure 5, we compare the Community-Consensus TSI composite with the other composites and with models during the spacecraft era (1978 to present day). The uncertainty in the Community-Consensus TSI composite grows in magnitude at the early part of the record, reflecting the poorer precision of the early radiometers (Dudok de Wit et al., 2017). The most distinguishing features of the comparisons are the growing discrepancies among the individual observation composites prior to the year 2000 as well as the growing divergence (secular trend) in the baseline irradiance of the SATIRE-S model and, to a lesser extent, the PMOD observations from the Community-Consensus TSI composite at consecutive solar minimum periods. The ACRIM composite differs most from the Community-Consensus TSI composite between 1990 and 2000.

SATIRE-S estimates of baseline irradiance levels at successive solar minima periods (i.e., interminima) are quite different from those by the NRLTSI2, NRLTSI3, and EMPIRE models. For example, SATIRE-S

Table 2
Solar Cycle TSI Energy Change for the Ascending and Descending Phases of Solar Cycles 23 and 24 During the SORCE TIM Era

Time periods (max, min)	Data set	ΔTSI (W/m^2)
Solar cycle 23 (descending phase)		
	SORCE TIM	0.603
Max: 5 Aug 2003–25 Oct 2003	PMOD	0.724
	RMIB	0.769
Min: 1 Nov 2008–1 Jan 2009	ACRIM	0.787
	NRLTSI2	0.553
	NRLTSI3	0.642
	SATIRE-S	0.658
	EMPIRE	0.603
Solar cycle 24 (ascending phase)		
	SORCE TIM	1.001
Max: 5 March 2014–25 May 2014	PMOD	0.805
	RMIB	0.757
Min: 1 Nov 2008–1 Jan 2009	ACRIM	-
	NRLTSI2	0.968
	NRLTSI3	0.918
	SATIRE-S	0.757
	EMPIRE	1.048
Solar cycle 24 (descending phase)		
	SORCE TIM	0.634
Max: 5 March 2014–25 May 2014	PMOD	0.586
	RMIB	-
Min: 5 March 2017–5 May 2017	ACRIM	-
	NRLTSI2	0.686
	NRLTSI3	0.565
	SATIRE-S	0.558
	EMPIRE	0.817

Note. The TSI values were computed from the difference of an average of TSI values for days in common among the data sets computed over the solar maximum and solar minimum time periods as reported in the table. Results are shown for three composites (PMOD, RMIB, and ACRIM), four models (NRLTSI2, NRLTSI3, SATIRE-S, and EMPIRE), and one observational record (SORCE TIM).

estimates a 1986–2008 TSI energy change of 0.5 W/m^2, a value that is approximately 40% of cycle 24 energy change (see Table 2), while the interminima estimates for the NRLTSI2, NRLTSI3, and EMPIRE models between 1986 and 2008 are smaller and range from 0.008 to 0.03 W/m^2. Interminima energy change in the Community-Consensus TSI composite between 1986 and 2009 is 0.03 $\pm$0.21 W/m^2 (Dudok de Wit et al., 2017), which is consistent with the NRLTSI2, NRLTSI3, and EMPIRE estimates. While the NRLTSI3 and NRLTSI2 models consistently have the smallest residual uncertainties with respect to the Community-Consensus TSI composite over the entirety of the spacecraft era (Figure 5d and Dudok de Wit et al. (2017)), the magnitude of the composite uncertainties precludes determining the best model among those shown. However, a temporal correlation analysis of the models with the Community-Consensus TSI composite shows that NRLTSI3 and NRLTSI2 have larger linear Pearson correlation coefficients than the EMPIRE and SATIRE-S models; this was also shown in Dudok de Wit et al. (2017).

The Community-Consensus TSI composite has a different 2008 solar minimum irradiance than the SORCE TIM observations but within the uncertainty of SORCE TIM (Figure 6a). The time-dependent residual difference of these two records can exceed 0.4 W/m^2 (Figure 6b), and reported uncertainties in the Community-Consensus TSI composite are lower than those reported for the direct SORCE TIM observations.

We conclude our TSI analysis by providing solar maximum-minus-minimum energy changes for time periods prior to the SORCE era (Table 3). The calculations are the difference of averages of daily irradiance values computed for days in common for the solar maximum and minimum time periods listed. From Table 3, we make the following generalized statements. Solar cycle energy changes in the PMOD composite and Community-Consensus TSI composite are generally smaller than in both RMIB and ACRIM. The largest solar cycle energy change of the observational data sets is reported in the ACRIM composite between 1979 and 1986 exceeding that of the other composites by more than 80%. At other time periods, RMIB consistently has the largest solar cycle variability of the composites. In the model data sets, EMPIRE consistently has the largest estimates of solar cycle energy change. Models typically agree in their solar cycle energy estimates to better than 10–20% with the exception of the descending phase of solar cycle 21 where the SATIRE-S estimate is lower than other models by upward of 30%. While all modeled solar cycle energy estimates fall within the upper range of values in the composites, the models sometimes fall outside the bounds on the lower range. For example, SATIRE-S during the descending phase of solar cycle 21 estimates lower cycle variability from the composites by upward of 20%. Likewise, in the ascending phase of solar cycle 23, NRLTSI3 predicts smaller solar cycle change than the composites by upward of 30% and NRLTSI2 and SATIRE-S to a smaller degree (~5%).

4. Comparisons of SSI Variability Models and Measurements

The relative influences of sunspots and faculae on solar irradiance change as a function of wavelength and the variations in total irradiance are the integral of wavelength-dependent variations in spectral irradiance. All models tend, in general, to show similar structure in spectral irradiance variability at rotational variability and solar cycle timescales reflecting temporal changes in the overall emergence, evolution, rotation across the Sun's disk projected to Earth, and disappearance of active regions during an approximate 11-year solar cycle. In this section, we compare the NRLSSI2 model with observations, observational composites, and independent models of SSI variability. As done for TSI in Section 3, these comparisons are made at solar rotational (Section 4.1) and solar cycle (Section 4.2) timescales using a variety of analyses approaches.

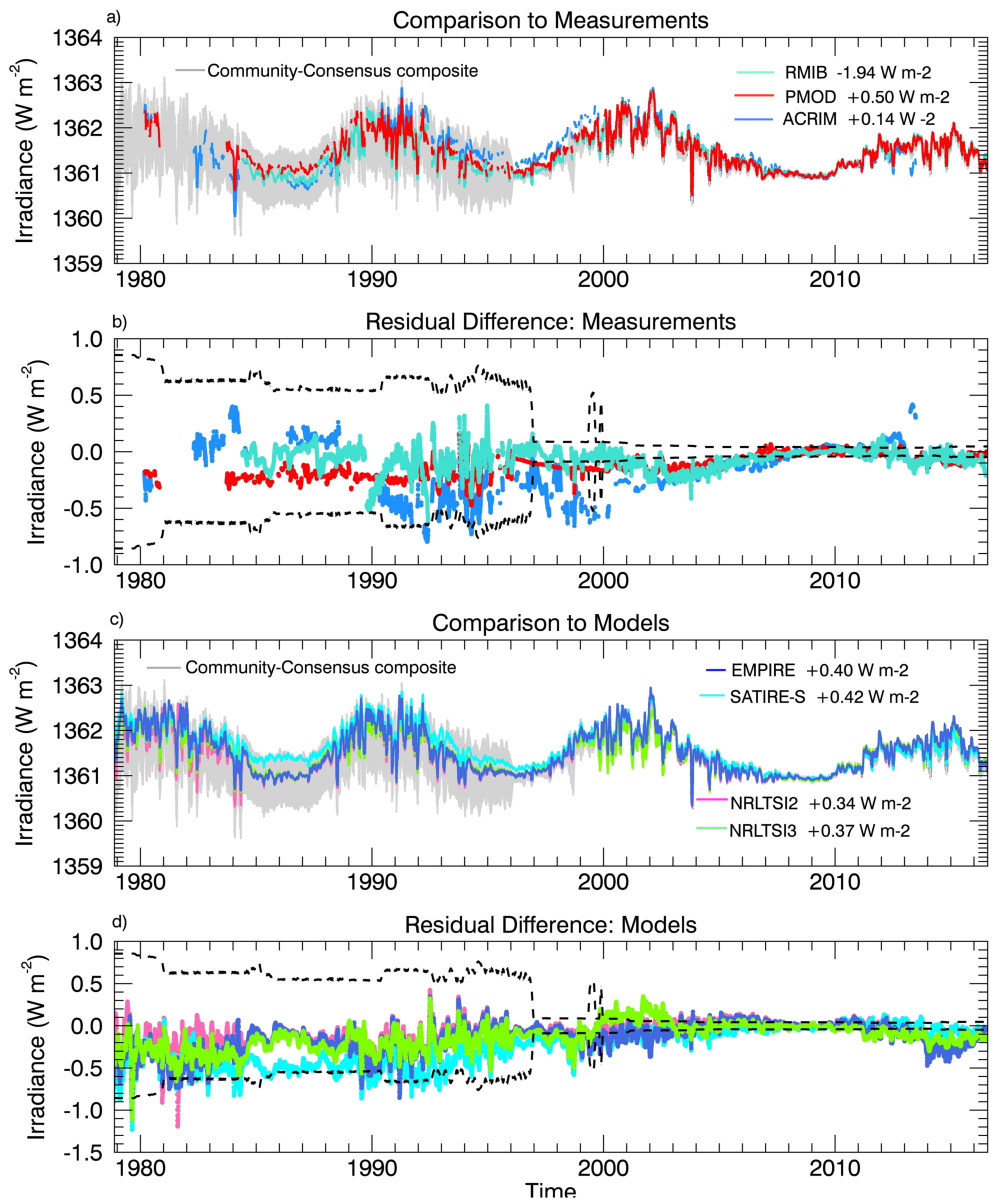

Figure 5. Measured and modeled TSI variability over the spacecraft era. Each data set has been smoothed with a 27-day running mean. (a) Time series comparisons of the ACRIM, PMOD, and RMIB TSI composites with the Community-Consensus TSI composite (grey shading reflects the uncertainty range of values). Due to differences in absolute scale, each composite has been normalized to the Community-Consensus TSI composite scale over an 81-day period centered on 1 September 2008; normalization values are provided in the legend. (b) Time series of residual differences with respect to the Community-Consensus TSI composite. Black dashed lines represent the +/−bounds of the time-dependent uncertainty in the Community-Consensus TSI composite. (c) As in (a) but for the NRLTSI2, NRLTSI3, SATIRE-S, and EMPIRE models. (d) As in (b) but for the NRLTSI2, NRLTSI3, SATIRE-S, and EMPIRE models.

We utilize a number of different data sets and models for our SSI comparisons. Observational data sets include SORCE SIM (J. Harder et al., 2005) and SOLSTICE (McClintock et al., 2005), a reanalysis of the SORCE SIM data set between 2004 and 2012, called constrained SIM (SIMc), that applies an alternative degradation model and differs from SORCE SIM data in long-term behavior (Mauceri et al., 2018), the OMI (Levelt et al., 2018; Marchenko & DeLand, 2014), and the Solar Irradiance Data Exploitation (SOLID) project SSI composite (Haberreiter et al., 2017). Models include a new NRL model version, NRLSSI3, and two independent solar irradiance models previously introduced: SATIRE-S and EMPIRE.

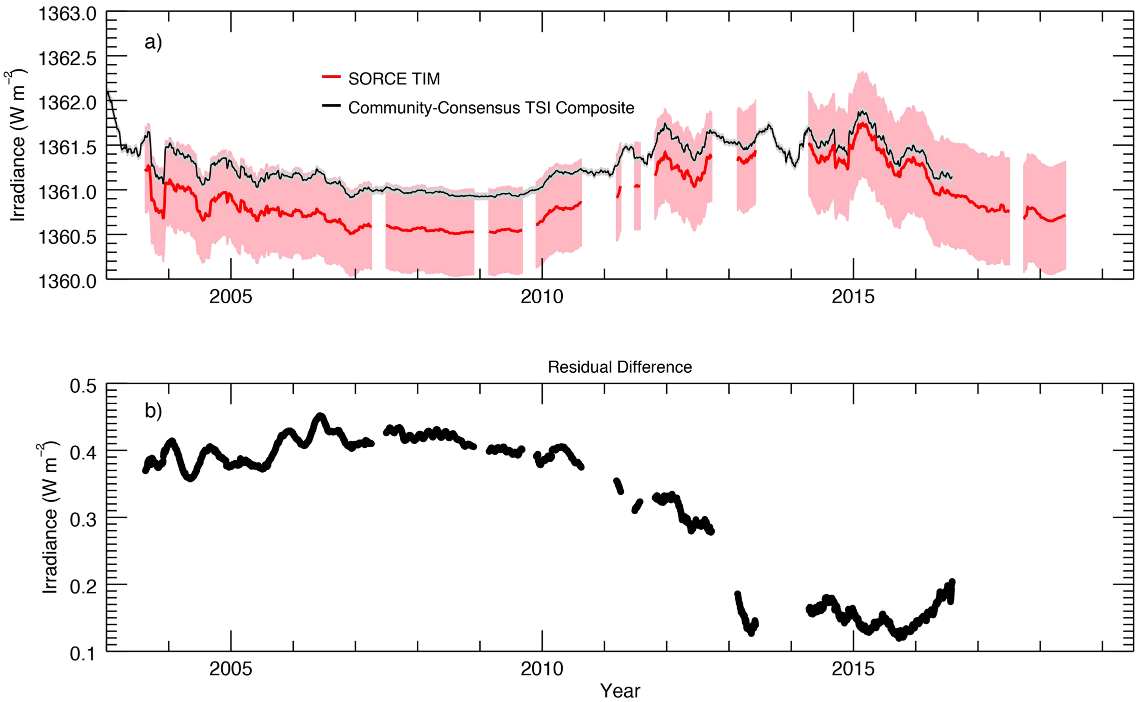

Figure 6. a) The Community-Consensus TSI composite (black with grey error bars) and the SORCE TIM observations (red with pink error bars) and (b) the residual difference. Data sets have been smoothed with an 81-day running mean.

A combined SORCE SIM (version 24) and SOLSTICE (version 16) level 3 daily product spanning 115 to 2400 nm is available from the SORCE website (http://lasp.colorado.edu/home/sorce/data/ssi-data/). We used data from file sorce_ssi_L3_c24h_0000nm_2413nm_20030301_20190114.txt in our analysis. This level 3 product utilizes SORCE SOLSTICE data below 310 nm and SORCE SIM data above 310 nm. In the websites https://sbuv2.gsfc.nasa.gov/solar/omi/ and http://lasp.colorado.edu/lisird/, OMI SSI data, specifically omi_ssi_update_20180510.h5, is publicly available. In the website ftp://ftp.pmodwrc.ch/pub/projects/SOLID/database/composite_published/, SOLID SSI composite is available.

The SOLID SSI composites are constructed using the approach of multiscale decomposition of the irradiance records, followed by a weighted average, and finally a recombination of the different scales (Haberreiter et al., 2017). To achieve this, it is a technical requirement that each individual irradiance record has the same temporal coverage and does not contain data gaps. Any data gaps are filled by applying the expectation maximization approach of Dudok de Wit et al. (2011) with a set of solar activity proxies. The composite is therefore not solely dependent on observations. However, when building the final composite, the newly added data points get a lower weight than the actual observations. Therefore, the overall variability of the SOLID composite can be considered as mainly driven by the observations. Haberreiter et al. (2017) further use a two-timescale proxy model to estimate the stability of that time series and identify patterns that cannot be reproduced by the model; this evaluation does not affect the actual SOLID SSI time series but the uncertainty assigned to it. At wavelengths below 420 nm, where the instrument spectral and temporal gaps from the multiple observations are smaller, the composite time series resembles weighted averages of the individual records. Conversely, at wavelengths above 420 nm, where SORCE SIM observations between Jan 2010 and Dec 2012 are the sole source of irradiance observations used to construct the composite, the expectation maximization approach largely determines the SSI time series and extends it in time.

The NRLSSI2 model also utilizes relationships between proxies and observed solar irradiance to model SSI variability at different wavelengths, but it is derived solely from SORCE SSI observations on rotational timescales. At decadal timescales, there is added uncertainty because of scaling the NRLSSI2 indices from rotational to solar cycle timescales. Therefore, at least at shorter wavelengths, the level of agreement or disagreement between NRLSSI2 and the SOLID SSI composite potentially enlightens our

Table 3
As in Table 2 But for the Time Period Prior to the SORCE Era and Also Including the Community-Consensus TSI Composite

Time periods (max, min)	Data set	ΔTSI (W/m^2)
Solar cycle 21 (descending phase)		
Max: 5 Oct 1979–25 Dec 1979	C-Consensus	0.864
	PMOD	0.827
Min: 5 Aug 1986–5 Oct 1986	RMIB	-
	ACRIM	1.573
	NRLTSI2	0.890
	NRLTSI3	0.752
	SATIRE-S	0.640
	EMPIRE	0.945
Solar cycle 22 (ascending phase)		
Max: 5 Oct 1989–25 Dec 1989	C-Consensus	1.047
	PMOD	1.054
Min: 5 Aug 1986–5 Oct 1986	RMIB	1.510
	ACRIM	1.474
	NRLTSI2	1.375
	NRLTSI3	1.222
	SATIRE-S	1.152
	EMPIRE	1.450
Solar cycle 22 (descending phase)		
Max: 5 Oct 1989–25 Dec 1989	C-Consensus	0.953
	PMOD	1.090
Min: 5 July 1996–25 Sept 1996	RMIB	1.401
	ACRIM	0.939
	NRLTSI2	1.283
	NRLTSI3	1.100
	SATIRE-S	1.337
	EMPIRE	1.353
Solar cycle 23 (ascending phase)		
Max: 5 Oct 2001–25 Dec 2001	C-Consensus	1.059
	PMOD	1.127
Min: 5 July 1996–25 Sept 1996	RMIB	1.255
	ACRIM	1.013
	NRLTSI2	0.966
	NRLTSI3	0.718
	SATIRE-S	0.986
	EMPIRE	1.074

understanding of SSI solar cycle irradiance variations because the proxy contribution to the SOLID SSI composite is reduced relative to the observational contribution. At longer wavelengths, however, the level of agreement or disagreement between NRLSSI2 and the SOLID SSI composite is more indicative of differences in the underlying methodologies that relate proxy variability to equivalent irradiance change; proxy reconstructions of SSI variability on solar cycle timescales have yet to be validated by the observations.

We note that while SORCE SSI data sets were utilized in the SOLID SSI composite as well as in the formulation of the NRLSSI2 model, the OMI and SIMc SSI data were not. Therefore, comparisons shown with OMI and SIMc provide independent validation of both the NRLSSI2 model and the SOLID SSI data set and methodology.

4.1. SSI on Solar Rotational Timescales

To isolate the Sun's rotational modulation of spectral irradiance, we detrend all measured and modeled time series by removing an 81-day running mean. Comparisons between the detrended NRLSSI2 model and the observations in five broad wavelength bands spanning 265 through 2000 nm are shown in the left-hand panel of Figure 7, while the right-hand panel compares the NRLSSI2 model to other models. Comparisons confirm that the NRLSSI2 model captures the physical behavior of sunspots and faculae. For example, a noticeable reduction in irradiance due to sunspot darkening near 2014.8, which is also evident in TSI in Figure 1, occurs in both SSI observations and the model at wavelengths longer than 310 nm but not at wavelengths shorter than 285 nm where enhancements due to facular brightening dominate.

Observations of SSI rotational variability agree to greater or lesser extents that may be attributed to different levels of observational noise. We derived an empirical noise estimate for the various observational data sets from the standard deviation of the absolute value of their rotational variability during 2008 when solar activity was minimal (not shown). The results indicate that OMI has better repeatability than SORCE SSI in the 265–285 nm and 310–340 nm bands. To be expected, SOLID SSI has better repeatability than OMI in the 310–400 nm band and better repeatability than SORCE SIM from 310–1000 nm, due to the stronger constraint by proxies in the SOLID composite at these wavelengths. We use this analysis as an empirical noise estimate to guide model validation throughout this section. In the UV band between 265 and 285 nm, the NRLSSI2 and NRLSSI3 models closely follow OMI rotational variability and SOLID SSI (in the smaller rotations); SATIRE-S rotational variability exceeds that of OMI and SOLID (in the smaller rotations), and rotational variability in the EMPIRE model exceeds that of observations with the highest noise. Between 310 and 400 nm, rotational variability in the EMPIRE model again exceeds that of all observations; other models also estimate larger variability than the low-noise OMI observations with NRLSSI2 to the least degree. Above 400 nm through the near-infrared, modeled rotational variability is mostly smaller than that of the SOLID SSI composite. As noted above, at wavelengths longer than 420 nm, SORCE SIM observations after 2010 provide the only observational source for the SOLID SSI composite (Haberreiter et al., 2017).

To better clarify SSI rotational variability, we determine the spectrum of rotational variability in 1-nm bins (Figure 8). These results are the 1-sigma standard deviation of the absolute value of the detrended rotational variability relative to the mean rotational variability. As expected, rotational modulation of solar irradiance is largest at the shortest wavelengths. Rotational variability at 150 nm is one order of magnitude larger than rotational variability at 300 nm and two orders of magnitude larger than rotational variability at 1600 nm. The rotational variability in the NRLSSI2 and NRLSSI3 models for wavelengths below 250 nm

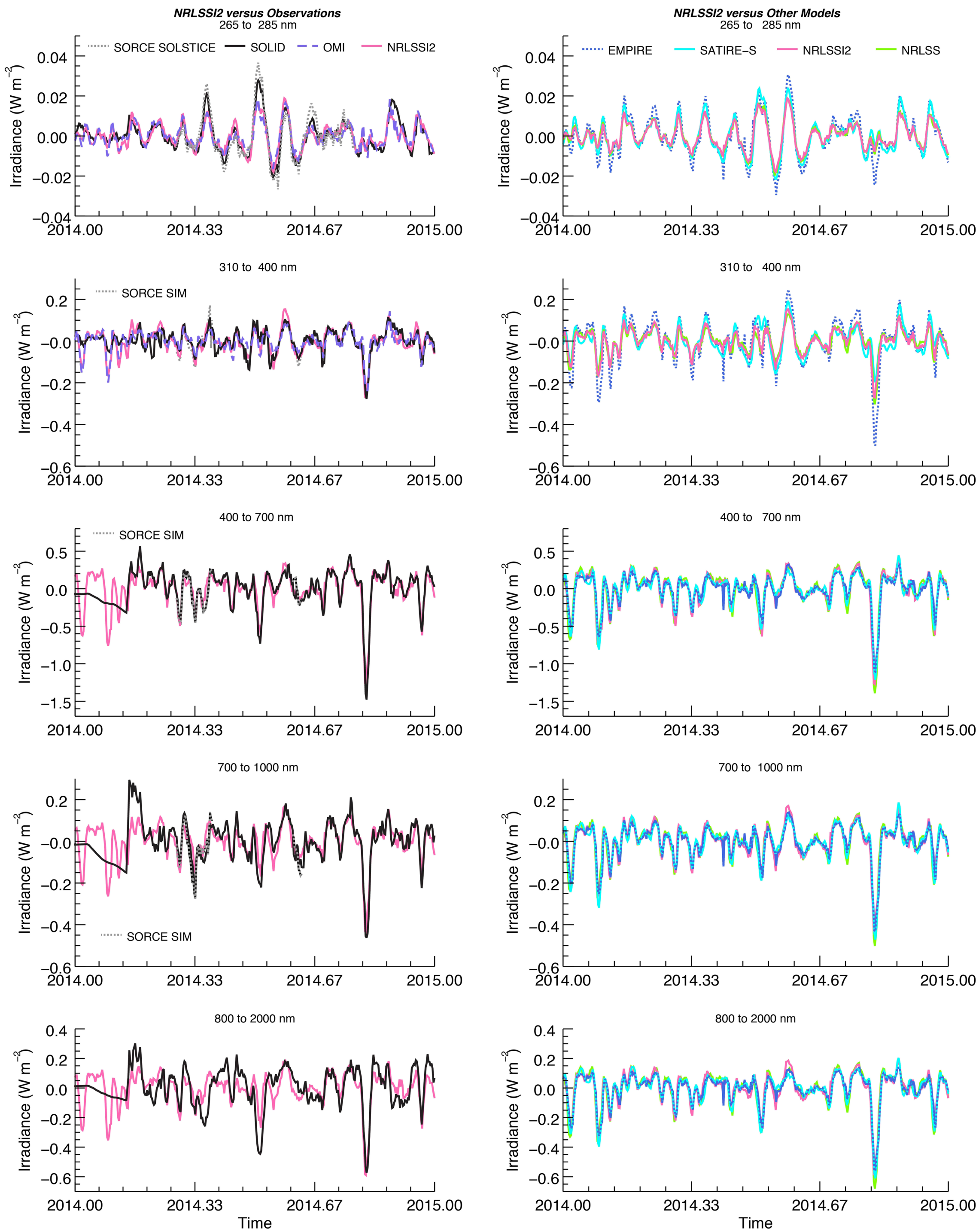

Figure 7. SSI rotational variability in five wavelength bands for the year 2014. Shown are comparisons of the NRLSSI2 model with SORCE and OMI observations and the SOLID SSI observational composite (left-hand panels) and of NRLSSI2 with independent models (right-hand panels). Rotational variability is derived by removing an 81-day running mean from each data set. SORCE SIM data is not shown for the 800–2000 nm integrated band because temporal gaps in the observations (occurring primarily at wavelengths above 1600 nm) preclude the 81-day detrending analysis. Comparisons to OMI cannot be made above its longest measurement channel of 500 nm. The y axis range of respective left and right panels is held fixed.

is very similar to that of SORCE SOLSTICE and larger than that of the SOLID SSI composite. At wavelengths below approximately 160 nm, rotational variability in EMPIRE and SATIRE-S exceeds that of all observations and the NRLSSI2 model. This is particularly true of the SATIRE-S model whose

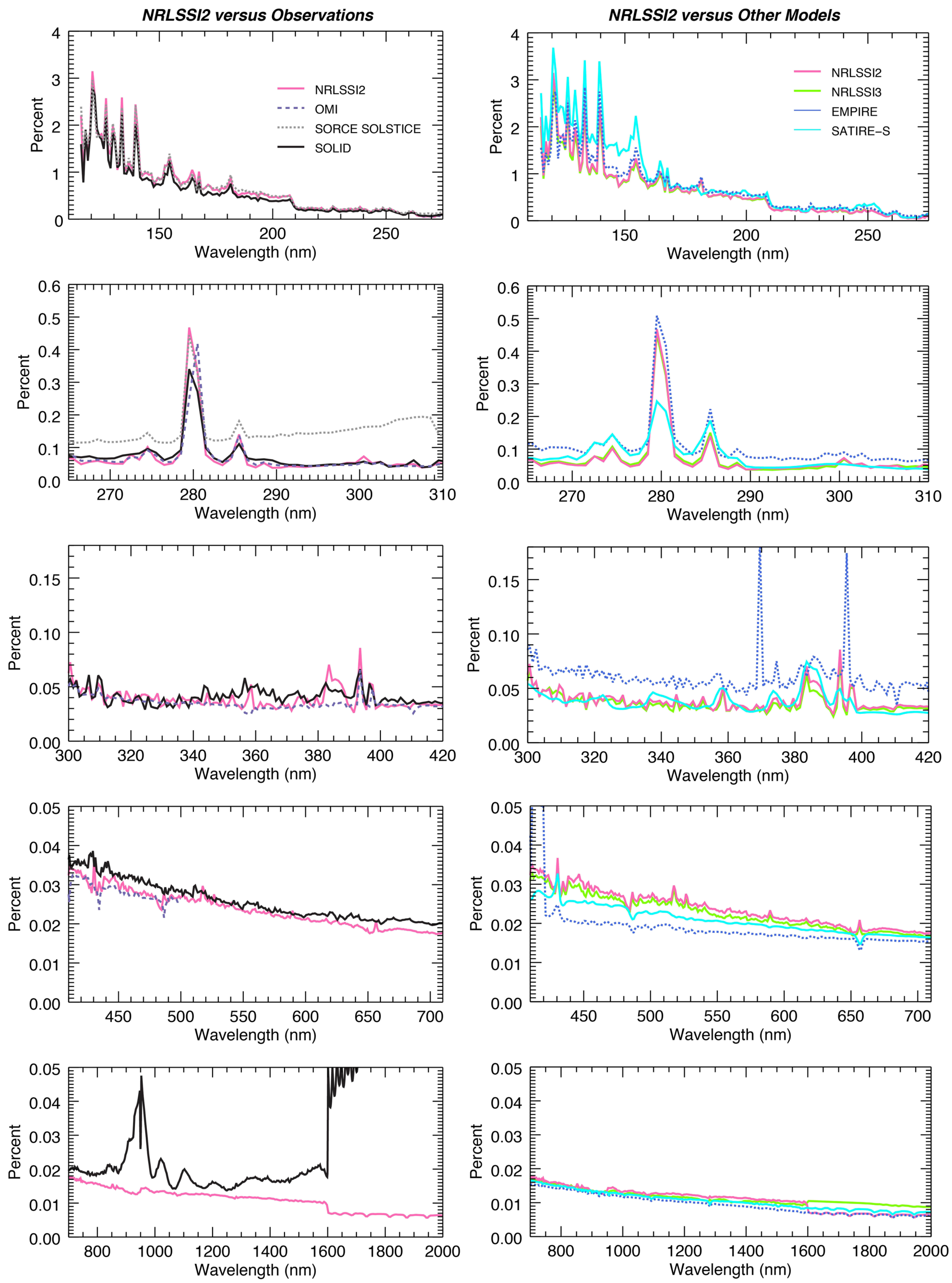

Figure 8. The spectrum of rotational variability in the NRLSSI2 model (pink) compared to the observational data sets (left column) and to the independent models (right column). Rotational variability has been isolated by removing an 81-day running mean from each data set. These results represent the 1-sigma standard deviation of the absolute value of the rotational variability relative to the mean rotational variability of each respective data set (reported in %). The results are specific to the time period 1 January 2011 to 31 December 2014 and have been computed for approximately 500 days in common overall data sets for wavelengths below 310 nm and around 1200 days in common for wavelengths longer than 310 nm. The y axis range of respective left and right panels is held fixed.

rotational variability can exceed observed variability by up to a factor of 1.8. Between 265 and 420 nm region, the rotational variability in NRLSSI2 and NRLSSI3 tracks OMI and the SOLID SSI composite, with the exception of the core of the Mg II line near 280 nm where NRLSSI2 and NRLSSI3 show more similarity to the SORCE SOLSTICE observations. Between 265 and 420 nm, rotational variability in

EMPIRE shares the same general spectral structure of NRLSSI2 and NRLSSI3 but with systematically larger magnitudes at all wavelengths. In contrast, the spectral structure of SATIRE-S differs from all observations and the other models. Specifically, the SATIRE-S rotational variability in core solar emission lines (e.g., 380 nm) exceeds that of the observations while, outside of core solar emission lines, the variability is similar to OMI, SOLID SSI, and the NRL models.

Above ~400 nm, the relative magnitudes of rotational variability in the models change respective to shorter wavelengths to ensure that the integral of SSI variability matches TSI rotational variability. The shift in SATIRE-S and EMPIRE from larger UV rotational variability (relative to the NRLSSI2 model) to smaller visible and near-IR rotational variability occurs at approximately 400 and 420 nm, respectively. At longer wavelengths, SATIRE-S and EMPIRE rotational variability is always smaller than NRLSSI2, NRLSSI3, and the SOLID SSI composite. Furthermore, the shift from larger UV variability to smaller visible and near-IR variability in EMPIRE is not a smooth transition, but rather a sudden, relative decrease of approximately 60%. Above 900 nm, and especially above 1600 nm, observed rotational variability is dominated by noise, and model validation is not possible at these wavelengths.

4.2. SSI on Solar Cycle Timescales

Comparisons of SSI variability during the 11-year solar cycle are far less definitive than during the 27-day rotations because of significant uncertainty in instrumental trends on multiyear timescales that may occur when the correction of instrumental artifacts, such as degradation, dominates observed solar cycle variability. For example, the analysis in this section shows that the SORCE SIM observational data set has solar cycle variability that can be out-of-phase with TSI at some wavelengths at some parts of the record but turn to in-phase with TSI at other parts of the record. This behavior is unique to SORCE SIM. Solar cycle variability in all other data sets is in-phase with TSI for the wavelength bands shown. Intermodel differences in solar cycle variability typically reflect similar differences in solar rotational variability. Solar cycle variability, like solar rotational variability, is strongly wavelength-dependent. Below 265 nm, solar cycle variability can reach and exceed 10% (DeLand et al., 2004; Meftah et al., 2016; Snow et al., 2010). Between 265 and 285 nm, solar cycle variability is on the order of 1%, decreasing to approximately 0.1% in the visible band between 400–700 nm (i.e., on the order of TSI solar cycle variability), to even less at near-infrared wavelengths.

Comparisons of measured and modeled SSI solar cycle variability for five broad, integrated, wavelength bins are shown in Figure 9. In the 265–285 nm integrated band, NRLSSI2 solar cycle variability is slightly larger than OMI, on par with SIMc, and smaller than SORCE SOLSTICE and the SOLID SSI composite, particularly in cycle 23. At 310–400 nm, NRLSSI2 cycle variability falls above OMI and SOLID SSI and below SIMc while SORCE SIM cycle variability is much larger. In the 400–700 nm visible band, NRLSSI2, SIMc, SOLID, and SORCE SIM show approximate agreement prior to ~2015. In the near-infrared, NRLSSI2 cycle variability is on par or less than that in the SOLID SSI composite and slightly larger than in SIMc. The magnitude and phasing of SSI solar cycle variability are generally similar in the different models but differ more among the observations with the exception being UV variability during the ascending phase of solar cycle 24 at 265–285 nm where disagreement in the model estimates is similar to that among various measurements.

We further quantify SSI solar cycle variability by tabulating energy change values for three separate periods during the SORCE era for the SORCE SIM and SOLSTICE instruments, the OMI instrument, and the NRLSSI2, SATIRE-S, and EMPIRE models (Table 4). SIMc is excluded from this analysis due to the shorter length of its record. The time periods selected for solar maximum and minimum activity are the same as those for which TSI solar cycle change values were previously computed (Table 2) such that interested readers may convert the SSI results from irradiance units into a percentage of TSI change.

From 2003 to 2014, solar cycle maximum-minus-minimum energy change in the 265–285 nm integrated band for SORCE SOLSTICE is larger than those for OMI and the SOLID SSI composite. During the descending phase of solar cycle 23 (i.e., 2003 to 2008), energy change in the 265–285 nm band for SORCE SOLSTICE and the SOLID SSI composite is also greater than all model estimates, which show more similarity with SIMc over its shorter record length. Beginning in 2008 (i.e., during solar cycle 24), modeled estimates of energy change in the 265–285 nm band by the NRLSSI2 and SATIRE-S models are in the range of the SORCE SOLSTICE and OMI observations, with NRLSSI2 estimates of energy change falling at the smaller end,

10.1029/2019EA000693

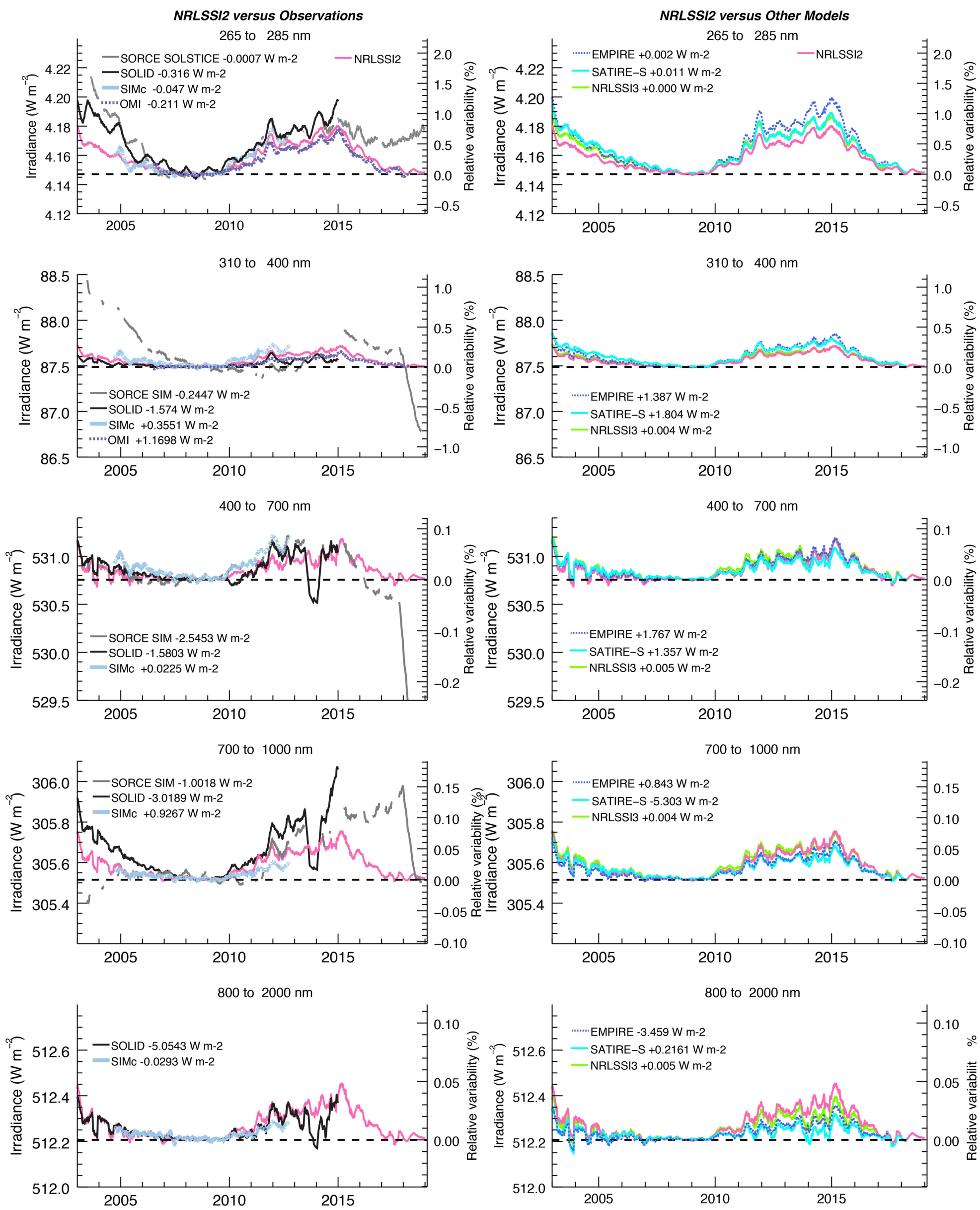

Figure 9. SSI solar cycle time series comparisons during the SORCE era. The comparisons of the NRLSSI2 model (pink) to observations and observational composites are shown in the left-hand column. The right-hand column, which maintains the same y axis scaling as the left-hand column, compares NRLSSI2 to other models. Each data set has been smoothed with an 81-day running mean. Due to differences in absolute scale, all data sets have been normalized to the NRLSSI2 value during solar minimum conditions (defined as the average of an 81-day period centered on 1 September 2008) using the offset factors reported in the legend. The right-hand y axis is the relative SSI variability (in %) with respect to the solar minimum reference period. The y axis in the 400–700 nm band has been truncated to aid visual comparisons; SORCE SIM values reach 528 W/m^2 in this wavelength band.

more similar to that of OMI, and the SATIRE-S estimates at the larger end, more similar to that of SORCE SOLSTICE. The energy change estimates by the EMPIRE model, for this same wavelength band and for the post-2008 time period, consistently exceed those of all observations. In the 310–400 nm integrated band, all models consistently estimate larger energy change values than the OMI observations or the SOLID SSI composite, and the overestimation is greatest for the EMPIRE model and smallest for the NRLSSI2 model. Here again, models show more similarity with SIMc over its shorter record length. At visible through near-infrared wavelengths, the NRLSSI2 model shows the best agreement with energy

Table 4
Solar Cycle SSI Energy Change in Five Integrated Wavelength Bins for the Ascending and Descending Phases of Solar Cycles 23 and 24

Time periods (max, min)	Data set	ΔSSI 265–285 nm ($W \cdot m^{-2}$)	ΔSSI 310–400 nm ($W \cdot m^{-2}$)	ΔSSI 400–700 nm ($W \cdot m^{-2}$)	ΔSSI 700–1,000 nm ($W \cdot m^{-2}$)	ΔSSI 800–2,000 nm ($W \cdot m^{-2}$)
Solar cycle 23 (descending phase)						
	SORCE SSI	0.062	0.759	0.075	−0.158	-
Max: 5 Aug 2003–25 Oct 2003	SOLID SSI	0.039	0.064	0.032	0.180	0.013
	NRLSSI2	0.016	0.045	−0.105	0.027	0.015
Min: 1 Nov 2008–Jan 2009	NRLSSI3	0.022	0.080	−0.028	0.047	−0.030
	SATIRE-S	0.029	0.192	0.053	0.049	−0.029
	EMPIRE	0.022	0.053	−0.022	0.006	−0.057
Solar cycle 24 (ascending phase)						
	SORCE SSI	0.044	0.294	0.575	0.349	-
Max: 5 March 2014–25 May 2014	SOLID SSI	0.040	0.181	0.302	0.436	0.272
	OMI	0.028	0.180	-	-	-
Min: 1 Nov 2008–Jan 2009	NRLSSI2	0.036	0.280	0.515	0.290	0.299
	NRLSSI3	0.042	0.277	0.465	0.258	0.202
	SATIRE-S	0.043	0.347	0.415	0.208	0.147
	EMPIRE	0.058	0.430	0.486	0.216	0.166
Solar cycle 24 (descending phase)						
	SORCE SSI	0.028	0.143	0.709	−0.030	-
Max: 5 March 2014–25 May 2014	OMI	0.031	0.175	-	-	-
	NRLSSI2	0.035	0.266	0.468	0.270	0.275
Min: 5 March 2017–5 May 2017	NRLSSI3	0.040	0.262	0.424	0.239	0.183
	SATIRE-S	0.040	0.320	0.356	0.180	0.121
	EMPIRE	0.052	0.381	0.447	0.199	0.153

Note. The ΔSSI values were computed from a difference of an average of integrated SSI values over the respective wavelength bins computed from days in common over the solar maximum and solar minimum time periods reported in the table. SORCE SIM ΔSSI values for the 800–2000 nm bin not provided due to data gaps. OMI results are available for a subset of this time period.

change values in the SOLID SSI composite during the descending phase of solar cycle 23 and with SORCE SIM observations and the SOLID SSI composite during the ascending phase of solar cycle 24 (i.e., 2008 to 2014). NRLSSI2 cycle variability is smaller than that of SIMc in the visible and larger than that of SIMc in the near-infrared.

In Figure 10, we extend time series comparisons of SSI solar cycle variability for the NRLSSI2, SATIRE-S, and EMPIRE models to encompass the spacecraft era. Solar cycle variability during the spacecraft era at UV through visible wavelengths is consistently the largest in the EMPIRE model and grows consecutively larger toward the start of the spacecraft era where EMPIRE irradiance estimates during solar maximum periods grow relative to the SOLID SSI composite and other models while still returning to approximately the same, baseline, irradiance values at solar minimum. In the near-infrared, the NRLSSI2 model has the largest solar cycle variability of the models over the spacecraft era, sometimes exceeding that of the SOLID SSI composite, and the SATIRE-S model has the least variability, even approaching negligible solar cycle variability in the descending phase of solar cycle 21 (i.e., 1979–1986).

The results in Figure 10 also indicate that the interminima (i.e., consecutive solar minima) trend in TSI evident in the SATIRE-S model (Figure 5) extends across the UV, visible and near-infrared spectrum; this interminimum behavior in SATIRE-S is not shared by the SOLID SSI composite or the NRLSSI2, NRLSSI3, and EMPIRE models. The interminima trend in the 1986 to 2008 minimum (i.e., from 5 August–25 October 1986 to 1 November 2008–25 January 2009) for the SATIRE-S model is 0.002, 0.167, 0.151, and 0.060 W/m^2 for 100–200, 200–400, 400–700, and 800–2,000 nm wavelength bands, respectively. Interminima trends in the SOLID SSI composite and the EMPIRE, NRLSSI2, and NRLSSI3 models for these same wavelength bands are smaller by about an order of magnitude.

In Table 5, we provide values of SSI solar cycle maximum-minus-minimum energy change values for the spacecraft era for the same time periods considered for TSI solar cycle energy change in Table 3. While all models tend to predict the same solar maximum minus solar minimum energy change to within 10–20% in the far-UV (100–200 nm) spectrum, the model estimates always exceed that of the SOLID SSI

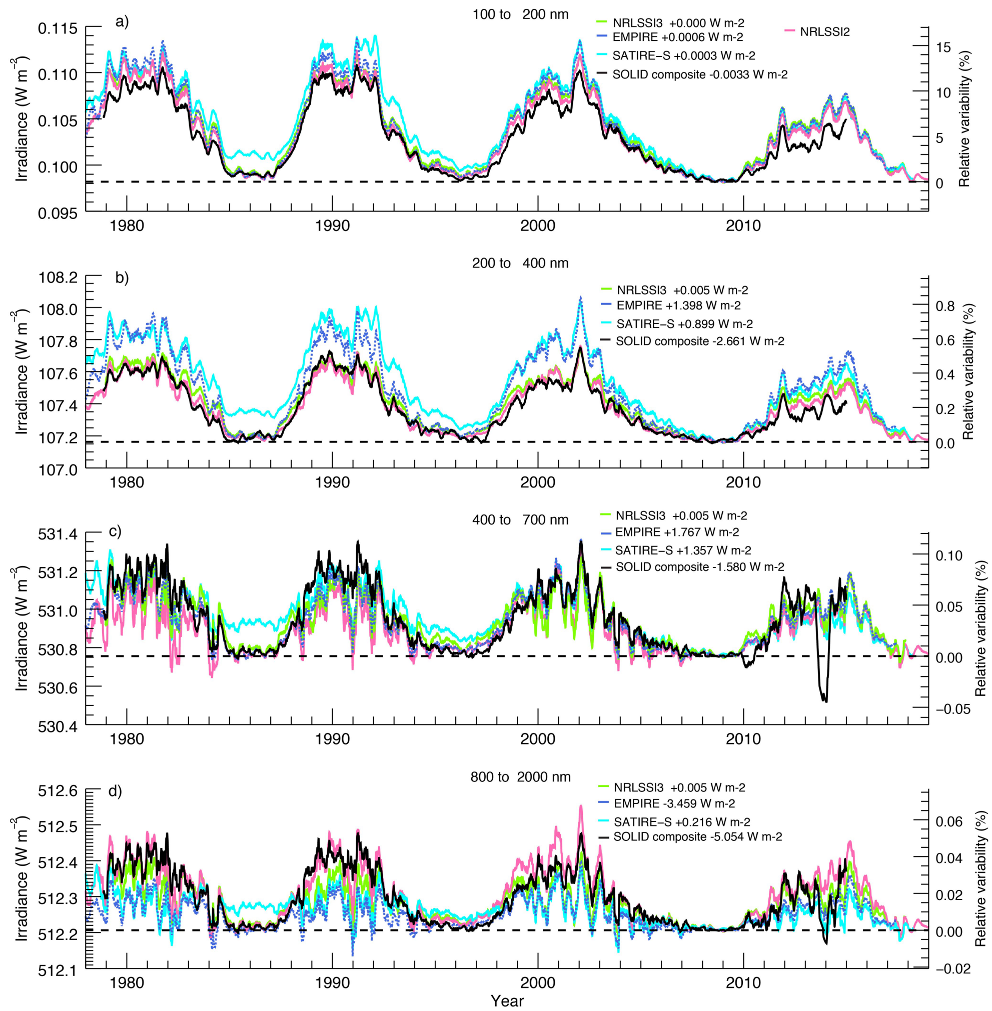

Figure 10. SSI solar cycle variability in the spacecraft era as estimated by models and integrated in broad UV, visible, and near-infrared wavelength bands. All data sets have been smoothed with an 81-day running mean. Due to differences in absolute scale, all data sets have been normalized to the NRLSSI2 value during solar minimum conditions (defined as the average of an 81-day period centered on 1 September 2008), and the legend provides the offset factors.

observational composite, and this is particularly true of the EMPIRE model. In the 200–400 nm integrated band, all models, but particularly EMPIRE, again exceed SOLID SSI cycle change by values up to 80%, and intermodel agreement is also poorer at 25–55% relative difference. In the visible through near-infrared, models also agree among each other to 10–50% but generally estimate smaller cycle variability than the SOLID SSI composite. The EMPIRE model tends to have larger cycle variability in the visible than the SATIRE-S and NRLSSI2 models. Intermodel differences in energy change estimates are greatest for the near-infrared wavelengths (800–2000 nm) and can reach relative differences of 80%.

5. Discussion

NOAA NCEI established the Solar Irradiance CDR in 2015 to provide ongoing specification of TSI and SSI on a range of timescales and over a broad range of wavelengths for the science community's use in assessing the Earth system response to solar variability. In this section, we discuss our analysis of the CDR performance and current understanding of solar irradiance variability on 27-day, solar rotational, timescales to decadal solar cycle variability and longer from comparisons of the CDR with observational data sets and independent models. Disagreements among the data sets highlight where future observations, new, improved composites, and future research are necessary to address limitations in our understanding of solar variability.

Table 5
As in Table 4 But for the Spacecraft Era and for Different Integrated Wavelength Bands

Time periods (max, min)	Data set	ΔSSI (W/m^2) 100–200 nm	ΔSSI (W/m^2) 200–400 nm	ΔSSI (W/m^2) 400–700 nm	ΔSSI (W/m^2) 800–2000 nm
Solar cycle 21 (descending phase)					
Max: 5 Oct 1979–25 Dec 1979	SOLID	0.008	0.332	0.620	0.291
Min: 5 Aug 1986–5 Oct 1986	NRLSSI2	0.010	0.392	0.267	0.188
	NRLSSI3	0.010	0.406	0.443	0.189
	SATIRE-S	0.009	0.449	0.210	0.037
	EMPIRE	0.011	0.528	0.361	0.096
Solar cycle 22 (ascending phase)					
Max: 5 Oct 1989–25 Dec 1989	SOLID	0.013	0.584	0.803	0.357
	NRLSSI2	0.016	0.711	0.668	0.413
Min: 5 Aug 1986–5 Oct 1986	NRLSSI3	0.015	0.690	0.728	0.315
	SATIRE-S	0.016	0.910	0.558	0.157
	EMPIRE	0.017	1.072	0.705	0.219
Solar cycle 22 (descending phase)					
Max: 5 Oct 1989–25 Dec 1989	SOLID	0.013	0.604	0.724	0.323
	NRLSSI2	0.015	0.668	0.554	0.354
Min: 5 July 1996–25 Sept 1996	NRLSSI3	0.014	0.635	0.575	0.244
	SATIRE-S	0.016	0.945	0.566	0.160
	EMPIRE	0.017	1.001	0.605	0.176
Solar cycle 23 (ascending phase)					
Max: 5 Oct 2001–25 Dec 2001	SOLID SSI	0.009	0.464	0.692	0.312
Min: 5 July 1996–25 Sept 1996	NRLSSI2	0.009	0.437	0.523	0.308
	NRLSSI3	0.009	0.431	0.483	0.209
	SATIRE-S	0.010	0.620	0.567	0.209
	EMPIRE	0.010	0.663	0.540	0.185

Note. Time periods for solar maximum and solar minimum match those for Table 3.

5.1. Sources of Solar Irradiance Variability

The NRLTSI2 and NRLSSI2 solar variability models, which specify irradiance for the NOAA Solar Irradiance CDR, determine variability in solar irradiance that occur with changes in solar magnetic activity from specified background, quiet Sun conditions that represent solar irradiance in the absence of magnetic activity. Furthermore, the models assume that bright faculae and dark sunspots are visible manifestations of this magnetic activity and use multiple linear regression to scale proxy indices of solar magnetic activity at any given time to equivalent irradiance change.

The scaling coefficients of the NRLTSI2 and NRLSSI2 models capture the relation of magnetic variability to variability in TSI and in the solar irradiance spectrum. The ability of the models to track observed variability during solar rotations verifies the models' formulation and coefficients, for example, that UV variability at wavelengths shorter than ~300 nm is affected solely by faculae, whereas irradiance at longer wavelengths is modulated by the net effect of spots and faculae (Frohlich & Lean, 2004). The NRLSSI2 scaling coefficients were derived from SORCE SOLSTICE and SIM SSI observations on solar rotational timescales alone to avoid introducing longer-term SORCE SSI instrumental trends into the NRLSSI2 model.

5.2. CDR Model Inputs and Operation

We verified the proxy inputs of facular brightening (i.e., the University of Bremen's Mg II index) and sunspot darkening (i.e., the USAF SOON network records of sunspot number area and location) through a series of numerical tests described in Coddington et al. (2016) that show the CDR has maintained stability since it was originally established in 2015. A year-by-year correlation analysis of the model inputs with independent proxies of solar activity shows long-term stability of the CDR's model inputs.

Since early 2015, there is a growing bias between the models (NRLTSI2 among others) and the SORCE TIM TSI observations that may suggest a problem in the model inputs, an issue with the SORCE TIM record, or a combination of both. Further analysis of the long-term stability of the CDR model inputs against independent records of facular brightening, particularly as solar magnetic activity increases with the beginning of the next solar cycle, is necessary. NASA's SIST activities to develop new and improved Mg II and Lyman-alpha (Machol et al., 2019) irradiance observational composites are expected to provide key new solar activity records in addition to the OMI and Bremen Mg II index records.

5.3. Solar Irradiance Variations on Solar Rotational Timescales

NRLTSI2, and all other models, on average reproduce observed SORCE TIM TSI variability over 27-day rotational periods to a high degree irrespective of differences in their underlying methodologies (Figure 1 and Figure 2). The SATIRE-3D model reproduces observed rotational TSI variability to the highest degree (to better than 0.3 W/m^2 residual difference as opposed to better than 0.5 W/m^2 for NRLTSI2, NRLTSI3, EMPIRE, and SATIRE-S) but may show a slight systematic enhancement of rotational TSI variability. Some potential reasons for this type of effect could include a small, systematic overestimation of the surface area of the magnetic features as they move across the Sun's disk as the Sun rotates or a systematic overestimation in the intensity of the quiet Sun or facular features that are obtained by radiative transfer calculations of 3-dimensional magnetohydrodynamic simulations of the solar atmosphere (Yeo, Solanki, et al., 2017). Future work could investigate the magnitude of the power in the rotational variability as a function of temporal periodicity using the periodogram analysis of Horne and Baliunas (1986) as demonstrated in Foukal and Lean (1986). Improvements in estimates of TSI rotational variability will benefit from the continuation of high-precision TSI and solar activity records.

NRLSSI2 spectral irradiance rotational variability between 265 and 500nm is validated by its good agreement with independent OMI observations (Figure 7 and Figure 8). Below 265 nm, NRLSSI2 rotational variability compares well with the SORCE SOLSTICE observations and the SOLID SSI composite, which includes contributions from a number of SSI instruments including SORCE SOLSTICE and SIM but not OMI (Haberreiter et al., 2017). Between 400 and 900 nm, NRLSSI2 rotational variability compares well with the SOLID SSI composite. Estimates of SSI rotational variability are essentially unconstrained by the extant observational records above 900 nm and particularly above 1600 nm (Figure 8) due to instrumental noise.

Other models of spectral irradiance variability agree less well with the OMI observations. SATIRE-S rotational variability below approximately 150 nm is systematically larger than the SOLID SSI composite and SORCE SOLSTICE observations by up to a factor of 1.8. Between 150 and 400 nm, SATIRE-S reproduces observed rotational variability in the wings of solar lines but not in the cores as seen, for example, in the elemental iron lines near 360 and 380 nm (Figure 8). There are two potential underlying sources for the SATIRE-S deficiencies. First, local thermodynamic equilibrium assumptions were used in the theoretical radiative transfer spectra to assign a unique intensity spectrum to different magnetic features (Unruh et al., 1999), but local thermodynamic equilibrium assumptions are invalid in the core of solar emission lines particularly at wavelengths below 300 nm (Krivova et al., 2006). Second, the SATIRE-S estimated irradiances between 115 and 180 nm are readjusted in a scaling to irradiance observations (Yeo et al., 2014).

Rotational variability in the EMPIRE model also differs notably from that of OMI observations, the SOLID SSI observational composite, and the NRLSSI2 model (Figure 7 and Figure 8) even though the EMPIRE model uses the same irradiance and solar proxy data sets as NRLSSI2 to derive its magnetic variability-to-irradiance relationships. EMPIRE UV rotational variability through 420 nm is too large relative to the observations, while the rotational variability at longer wavelengths is too small.

There are differences between the SATIRE and EMPIRE models themselves, in addition to their differences from the OMI and other observations, which contradict prior assertions (Yeo, Krivova, et al., 2017) that their mutual consistency supports larger UV variability than is evident in the NRLSSI2 model. The spectral character of rotational variability in the EMPIRE model is found to differ systematically from that of the SATIRE-S model and to have a discontinuous spectral transition around 420 nm (Figure 8). Furthermore, Yeo et al. (2017) claim that the NRLSSI2 model was affected by "regression attenuation" (i.e., a dampened response) because it uses ordinary least squares (OLS) regression to relate magnetic variability to irradiance change as opposed to the orthogonal distance regression (ODR) approach like the EMPIRE model employs. OLS and ODR are both statistical linear regression approaches. OLS considers errors in the irradiance observations during the regression analysis, and ODR considers errors in the irradiance observations and the solar proxies; in the absence of error in the proxies, ODR converges to the OLS result. A common misapplication of ODR is the exaggeration of measurement errors leading to an overestimate of the slope of the linear regression that relates physical quantities (i.e., a heightened response) (Carroll & Ruppert, 1996). Potentially, the too large UV variability in the EMPIRE model is the result of an incorrect assignment of measurement errors in the ODR application. Errors in the proxy inputs of facular brightening and sunspot darkening are not well quantified and, typically, are estimated from time series differences and correlation studies with independent records (Coddington et al., 2016; Yeo, Krivova, et al., 2017) that are affected by their own set of underlying and poorly quantified uncertainties. Additionally, a sensitivity analysis of a TSI proxy model to OLS and ODR methodologies has established that the OLS and ODR regression approaches gave identical TSI estimates when the assigned proxy errors for facular brightening and sunspot darkening were equal and no larger than 10%; at higher uncertainties, the facular brightening coefficient became more sensitive to larger error than the sunspot darkening coefficient (McComas & Coddington, 2018). Future work to better quantify measurement error will benefit empirical solar irradiance modeling. The empirically derived noise estimate we used to guide model validation of SSI rotational variability may be imperfect, potentially misclassifying variability in a data set collected at high temporal cadence and followed by daily averaging (i.e., SORCE SOLSTICE) as noise relative to a data set collected approximately once per day (i.e., OMI). Furthermore, SSI observations of sufficient repeatability and accuracy, such as those expected from TSIS-1 SIM, are necessary to validate estimates of SSI rotational variability at visible through near-infrared wavelengths and to address the validity of the assumption of a linear relationship between magnetic variability and irradiance change.

5.4. Solar Irradiance Variations on Solar Cycle Timescales

On decadal timescales, the most noticeable difference between different model estimates and TSI observations is a secular trend in the SATIRE-S irradiance estimates that is not evident in the SORCE TIM observations or the NRLTSI2 and EMPIRE models (Figure 3). The secular trend may reflect that the magnetograms used in the SATIRE-S methodology (Yeo et al., 2014) do not have the necessary stability to produce long-term irradiance prior to 1996, when the inputs for the SATIRE model rely on ground-based, rather than space-based magnetograms. Wang and Sheeley (2015) show that estimates of the open solar magnetic flux computed from two different ground-based magnetogram records differ in magnitude and over time. Due to its shorter record length, the SATIRE-3D model performance on decadal timescales and longer cannot yet be assessed. Continued, high-accuracy, high-stability solar irradiance and magnetogram observations are necessary to validate estimated decadal-scale and longer TSI variability.

Since approximately 2016, the SORCE TIM observations show a high bias in TSI relative to all models at around the 0.01–0.02 W/m^2 level. Further research is required to ultimately diagnose the source, or sources, of this bias, which could originate in the observations, the models, or a combination of both. The 1- to 2-year drift between nearly identical TIM instruments on the SORCE and TCTE platforms (Figure 4) exceeds stability requirements and suggests there are, at a minimum, instrumental effects in one or both of these TIM TSI records that are not yet fully understood. Such drifts exemplify the challenge in producing highly-stable long-term instrumental records even when different instruments share the same design and data processing software.

Differences across observation-based composites of the 40-year extant TSI database can exceed 0.5 W/m^2, and their respective reconstructions of irradiance change between solar maxima and minima periods over the past 3.5 solar cycles can differ by up to 80% (Figure 5 and Table 3). The differences between the TSI composites, which vary in their creation approach, are larger in the earlier part of the space era than present day. NRLTSI2 and NRLTSI3 estimates between 1978 and present day reproduce the Community-Consensus TSI composite better than any other model, as determined by the smallest mean residual difference and the largest temporal correlation coefficient. The secular trend in the SATIRE-S model is evident throughout the space era and is not evident in the Community-Consensus TSI composite. The SATIRE-S estimates fall within the uncertainties of the Community-Consensus TSI composite, even in solar cycle 21, where the divergence between these records is greatest and reflects the large uncertainties in the composite in the early years of the spacecraft record because of the poorer precision of the early radiometers.

The Community-Consensus TSI composite during the SORCE era diverges from the direct, high-accuracy, SORCE TIM observations (Figure 6), which are also the most precise and inherently stable records in the extant TSI database (Kopp, 2014). The Community-Consensus TSI composite methodology provides a weighted average of available instrument records based on data-derived metrics of short-term instrument precision; the methodology cannot diagnose or correct instrument artifacts that may contaminate long-term instrument stability (Dudok de Wit et al., 2017). As such, the extent to which the Community-Consensus TSI composite can assuage disagreements about the accuracy of different long-term trends in the observational TSI records, for example, as shown in Figure 3a for the SORCE TIM and PMOD records, is unclear given that it differs in a time-dependent way from the SORCE TIM observations. A valuable future research contribution would be the incorporation of inherent instrument stability metrics in the development of a TSI composite. For the best quality empirical TSI proxy model, the combination of high-precision and high-stability irradiance observations is necessary, and analysis performed for the version 3 NRL models have shown that the direct SORCE TIM observations outperform the Community-Consensus TSI composite for this purpose.

SSI solar cycle variability in OMI, SIMc, the direct SORCE SOLSTICE and SIM observations, and the SOLID SSI composite differ substantially from each other and typically by more than model estimates differ from each other (Figure 9). The differences reflect the challenge in measuring the spectrum of the Sun over long time periods where the level of corrections for instrument artifacts, such as degradation, may exceed solar cycle variability. The OMI and SORCE SSI instruments use a different set of approaches and assumptions to correct for degradation. The time-dependent degradation in the OMI SSI record is detected and corrected according to an assumption that any trends in the irradiance record during minima in solar activity are instrumental artifacts (Marchenko & DeLand, 2014). The latest version of the OMI SSI data (Marchenko et al., 2019), as shown in this paper, relies on a more refined degradation model that links adjacent solar minima. Conversely, degradation correction for the SORCE SOLSTICE instrument is based on periodic comparisons between observed solar irradiance and an ensemble of stable stars that form a calibration reference over century timescales (Snow et al., 2005). SORCE SIM applies a still different degradation correction approach that is based on periodic comparisons of solar irradiance observations made from a primary channel with a less frequently used back up channel (Harder et al., 2009), thus refining the initial procedure that involved a direct prism transmission calibration of the two channels (Harder et al., 2005). The SIMc data set uses SORCE TIM observations to construct an alternative degradation model to the duty-cycle approach of the direct integrated SORCE SIM observations (Mauceri et al., 2018). Observed SIMc and OMI solar cycle variability between 265 and 500 nm is smaller than that of SORCE SOLSTICE and SIM.

The phasing of the solar cycle variability in SORCE SIM observations also differs from the other observational data sets (Figure 9). For example, near-infrared SORCE SIM variability is out-of-phase with respect to TSI variability during some periods of the solar cycle but is in-phase at other periods. The solar cycle variability in SIMc and also in the SOLID SSI composite, for which SORCE SIM provides the only observational source at wavelengths longer than 420 nm (Haberreiter et al., 2017), is always in-phase with TSI solar cycle variability. We note, however, that only a subset of the SORCE SIM data from 1 January 2010 to 31 December 2012, that is, the timeframe for which data showed an in-phase variability with the solar cycle, was used in the SOLID composite. The short time period of the SIM data along with the fact that the SIM data has a high noise level poses a challenge for constructing the SOLID composite at the visible and IR wavelengths. A revised SOLID composite is currently in preparation to improve the temporal extension of the SORCE SIM data set in the composite. All models also have a SSI solar cycle variability that is in-phase with TSI for the integrated bands shown. Continued and improved OMI observations and the new high-stability SSI observations now being made by TSIS-1 SIM (followed into the future by TSIS-2 SIM, etc.) will provide valuable information about SSI solar cycle variability for model validation. TSIS-1 SIM differs, in part, from SORCE SIM by the introduction of a third independent channel, which will be exposed infrequently to reduce degradation correction uncertainties (Richard et al., 2011; Richard et al., 2014).

In both the NRLSSI2 and SATIRE-S models, the structure of the wavelength dependence of the irradiance variability during solar rotation is similar but smaller in magnitude during the solar cycle. This is consistent with our understanding that faculae and sunspots are the common causes of variability on both timescales such that a larger (smaller) rotational variability at a particular wavelength or wavelength band in one model relative to the other is accompanied by a larger (smaller) solar cycle variability at that same wavelength or wavelength band. The EMPIRE model, however, does not always have this general characteristic of the NRLSSI2 and SATIRE-S models since in the 400–700 nm integrated band, this model has smaller rotational variability than either NRLSSI2 or SATIRE-S models (Figure 7) but sometimes greater solar cycle variability (Table 5). Future work could establish any role of the discontinuous drop in the EMPIRE rotational variability from large variability just short of 420 nm to small variability just long of 420 nm plays in these results.

The EMPIRE model has consistently the largest solar cycle variability of all models in the UV and visible wavelengths during the spacecraft era, especially in the earliest years of the space-based record (Figure 10 and Table 5). The SATIRE-S model is unique among both models and observations in that it has a secular trend in TSI and across the spectrum from far-UV to near-infrared wavelengths (Figure 10) over the 40-year duration of space-based irradiance observations. In the descending phase of solar cycle 21, near-infrared solar cycle variability in the SATIRE-S model is negligible.

Solar irradiance estimates from models, such as NRL and SATIRE, are used in climate models to assess the solar forcing impacts on Earth's climate. The original NRLTSI and NRLSSI models were used to specify solar forcing in the fifth Coupled Model Intercomparison Project (CMIP5). For the sixth Coupled Model Intercomparison Project (CMIP6), Matthes et al. (2017) recommended the use of the arithmetic average of the NRLTSI2/NRLSSI2 and SATIRE models. CMIP6 climate model simulations of responses to solar forcing resulted in enhanced shortwave heating and temperatures at the stratopause and enhanced ozone concentrations in the tropical upper stratosphere relative to CMIP5 solar forcing; the results were not statistically significant except for wavelengths between 300 and 350 nm, which is a region important for ozone chemistry. By extension, the enhancements of the climate impacts when adopting the SATIRE-S solar forcing alone would be even larger than seen for CMIP6 and differ even more from CMIP5. A companion paper in preparation further discusses difference between the NRL family of models (version 2 and version 3) and the SATIRE-S model.

Matthes et al. (2017) justified using the average of NRLTSI2/NRLSSI2 and SATIRE as the solar forcing in CMIP6 because of a lack of consensus about the performance of these models at that time. Since then, as this paper shows, new observation-based data sets have provided key new insights about model performance. In particular, 27-day rotational variability between 265 and 500 nm in the NRLSSI2 model has been validated by observations of 27-day solar rotations made independently by the OMI and shows enhanced performance relative to SATIRE-S. Second, a greater temporal correlation of the NRLTSI2 model with the Community-Consensus TSI composite over the spacecraft era relative to the correlation of SATIRE-S with the composite has been found; all models, however, fall within the magnitude of the irradiance uncertainties in the Community-Consensus TSI composite. Third, it appears that the long-term downward interminima trend in the SATIRE model during the space era is absent in all other models and observational composites of both total and spectral irradiance variability. More generally, our comparisons of solar energy change at all solar maxima and minima periods (e.g., Table 2 through Table 5) across the spacecraft era provide valuable insight for climate modelers who may be interested in assessing whether a single solar cycle is reflective of the magnitude of solar cycle forcing at other solar cycles and the implications of that choice for their results.

5.5. Continuing and Improving the Solar Irradiance CDR

Extending the Solar Irradiance CDR into the future relies on timely, ongoing availability of the model inputs of facular brightening (i.e., the University of Bremen's Mg II record) and sunspot darkening (i.e., the USAF SOON network of sunspot area and location data). We anticipate using the operational Mg II index from GOES-R as a proxy of facular brightening to complement the Bremen Mg II index composite, which is a research product. To ensure rapid availability of all ten SOON stations that we use to calculate the sunspot darkening index, LASP plans to become an archival server of the USAF SOON station records.

Efforts are underway to improve and extend the utility of the NRLTSI2 and NRLSSI2 models in three key ways: better sunspot darkening and facular brightening functions, adopting a higher-accuracy quiet Sun reference spectrum, and producing a higher spectral-resolution model. Identified improvements in the NRL models will ultimately transition to a future version of the Solar Irradiance CDR. For example, sunspot data in the Debrecen Heliophysical Observatory provides an independent database for validating and improving the sunspot darkening index calculated from the USAF SOON network. Extension of the CDR prior to 1978 requires reliable cross-calibration of the SOON and Debrecen sunspot data with the historical observations made by the RGO to verify the scaling adopted for v02r00 CDR and reconciliation of the sunspot number record (Clette et al., 2014; Clette et al., 2015). A further improvement is incorporation of the most reliable absolute spectral irradiance scale based on TSIS-1 SIM observations that differ in some wavelength regions from the WHI reference spectrum currently adopted.

New irradiance data sets, in particular the TSIS observations that commenced in 2018, will facilitate multiple aspects of future needs, especially for better understanding of spectral irradiance variability and improving the models that the CDR utilizes. New and improved composites of solar irradiance and solar activity, including those from SIST, are extended in time and facilitate new models of solar irradiance variability for climate research. These include an extension of an SSI composite methodology for longer time periods and incorporate improved, time-extended OMI data with additional SSI data sets (DeLand et al., 2019), a new version of the Mg II composite, in preparation, a new version of the Lyman-alpha irradiance composite (Machol et al., 2019), and the new Community-Consensus TSI composite. Additional reanalysis of existing data sets is also being performed, using, for example, the MUltiple-Same-Irradiance-Level technique, to correct the long-term SORCE SSI record (Woods et al., 2018). MUltiple-Same-Irradiance-Level corrects the long-term SORCE SSI record from the SOLSTICE and SIM instruments (and other SSI records) for uncorrected instrument degradation by relating 27-day smoothed irradiance values for each wavelength at pre- and postsolar minimum times to similar levels of solar activity as represented by a 27-day smoothed "super-proxy." The super-proxy is the average of sunspot number, Lyman-alpha irradiance, Mg II index, and the F10.7 cm radio flux after each record is separately normalized from 0 (cycle minimum value) to 100 (cycle maximum value).

6. Summary

In this work, we establish the consistency between the NRLTSI2 and NRLSSI2 models of solar irradiance with the observational record and other models and thereby establish the utility of these models for Earth atmospheric and climate science studies and their use in the NCEI Solar Irradiance CDR. We validate NRLTSI2 on rotational timescales and over a solar cycle against SORCE TIM observations. NRLTSI2 estimates over the spacecraft era have high temporal correlation with, and agree in magnitude to, the Community-Consensus TSI composite. NRLSSI2 estimates of UV rotational variability compare well with rotational variability in the observations from SORCE SOLSTICE, OMI, and the SOLID SSI composite. Between 265 and 500 nm, NRLSSI2 rotational variability is validated by its good agreement with the independent OMI observations. At longer visible through near-infrared wavelengths (<900 nm), NRLSSI2 rotational variability also compares well with rotational variability in the SOLID SSI composite. Above 900 nm, and particularly above 1600 nm, noise in the instrumental records precludes model validation. On solar cycle timescales, observational data sets differ from each other to a degree that matches, or exceeds, the differences between the various models, thus precluding model validation. SSI variability remains relatively unconstrained by the observational records at time periods longer than a few solar rotations, particularly at visible through near-infrared wavelengths. Continuation of space-based data sets is essential for improving our current knowledge of solar irradiance variability. New and improved data sets are expected to provide key information of SSI variability over extended time and spectral ranges, for example, TSIS-1 and OMI.

New and improved capabilities that are guided by new and improved observational databases, such as sunspot darkening and facular brightening indices, a higher accuracy reference spectrum, and higher spectral resolution, are under development for the NRL/LASP family of models. These improvements will ultimately be incorporated into a future version of the Solar Irradiance CDR.

Acknowledgments
We gratefully acknowledge the support by the NOAA Climate Data Record Program and the NASA Solar Irradiance Science Team. Additionally, we acknowledge the detailed and ongoing efforts of many people in providing and maintaining the observational irradiance and solar activity data sets that we used in our analysis. Some of these people are coauthors on this paper. For the many others, we recognize the efforts of the following individuals and groups as we used their data and models in our analysis: Natasha Krivova and Kok Leng Yeo of the Max Planck Institute for Solar System Research for the SATIRE-S, EMPIRE, and SATIRE-3D models; the SORCE and OMI science and data processing teams; the PMOD, ACRIM, and RMIB TSI composite science teams; the many individuals participating in the first European SOLID project; Mark Weber of the University of Bremen; the USAF SOON network; and the helpful assistance with SOON data access by the people in the NCEI/Boulder office. Finally, we also acknowledge two anonymous reviewers, whose comments and suggestions greatly improved our manuscript. The data supporting the findings of this study are in repositories as indicated within the article. This work was supported by the NOAA Climate Data Record Program and NASA Solar Irradiance Science Team under Grant Numbers NNX15AK59G and 80NSSC18K1304. M. H. acknowledges funding by Daniel Karbacher.

References

Bates, J. J., & Privette, J. L. (2012). A maturity model for assessing the completeness of climate data records. *Eos Transactions, American Geophysical Union*, *93*(44). https://doi.org/10.1029/2012eo440006

Bates, J. J., Privette, J. L., Kearns, E. J., Glance, W., & Zhao, X. P. (2016). Sustained production of multidecadal climate records: Lessons from the NOAA Climate Data Record Program. *Bulletin of the American Meteorological Society*, *97*(9), 1573–1581. https://doi.org/10.1175/Bams-D-15-00015.1

Carroll, R. J., & Ruppert, D. (1996). The use and misuse of orthogonal regression in linear errors-in-variables models. *American Statistician*, *50*(1), 1–6. https://doi.org/10.2307/2685035

Chapman, G. A., Cookson, A. M., & Dobias, J. J. (1997). Solar variability and the relation of facular to sunspot areas during solar cycle 22. *Astrophysical Journal*, *482*(1), 541–545. https://doi.org/10.1086/304138

Clette, F., Cliver, E. W., Lefevre, L., Svalgaard, L., & Vaquero, J. M. (2015). Revision of the sunspot number(s). *Space Weather-the International Journal of Research and Applications*, *13*(9), 529–530. https://doi.org/10.1002/2015sw001264

Clette, F., Svalgaard, L., Vaquero, J. M., & Cliver, E. W. (2014). Revisiting the sunspot number: A 400-year perspective on the solar cycle. *Space Science Reviews*, *186*(1-4), 35–103. https://doi.org/10.1007/s11214-014-0074-2

Clough, S. A., Iacono, M. J., & Moncet, J. L. (1992). Line-by-line calculations of atmospheric fluxes and cooling rates—Application to water-vapor. *Journal of Geophysical Research-Atmospheres*, *97*(D14), 15,761–15,785. https://doi.org/10.1029/92jd01419

Clough, S. A., Shephard, M. W., Mlawer, E., Delamere, J. S., Iacono, M., Cady-Pereira, K., et al. (2005). Atmospheric radiative transfer modeling: A summary of the AER codes. *Journal of Quantitative Spectroscopy & Radiative Transfer*, *91*(2), 233–244. https://doi.org/10.1016/j.jqsrt.2004.05.058

Coddington, O., & Lean, J. (2015). Climate algorithm theoretical basis document: Total solar irradiance and solar spectral irradiance. Retrieved from http://www1.ncdc.noaa.gov/pub/data/sds/cdr/CDRs/Solar Spectral Irradiance/AlgorithmDescription.pdf

Coddington, O., Lean, J. L., Pilewskie, P., Snow, M., & Lindholm, D. (2016). A solar irradiance climate data record. *Bulletin of the American Meteorological Society*, *97*(7), 1265–1282. https://doi.org/10.1175/Bams-D-14-00265.1

DeLand, M., & Marchenko, S. (2013). The solar chromospheric Ca and Mg indices from Aura OMI. *Journal of Geophysical Research:-Atmospheres*, *118*(8), 3415–3423. https://doi.org/10.1002/jgrd.50310

DeLand, M. T., Cebula, R. P., & Hilsenrath, E. (2004). Observations of solar spectral irradiance change during cycle 22 from NOAA-9 solar backscattered ultraviolet model 2 (SBUV/2). *Journal of Geophysical Research-Atmospheres*, *109*(D6), D06304. https://doi.org/10.1029/2003jd004074

DeLand, M. T., Floyd, L. E., Marchenko, S., & Tiruchirapalli, R. (2019). Creation of the GSFCSSI2 Composite Solar Spectral Irradiance Data Set. *Earth and Space Science*, *6*(7), 1284–1298. https://doi.org/10.1029/2019EA000616

Dewitte, S., & Nevens, S. (2016). The total solar irradiance climate data record. *Astrophysical Journal*, *830*(1), 25. https://doi.org/10.3847/0004-637x/830/1/25

Dudok de Wit, T. (2011). A method for filling gaps in solar irradiance and solar proxy data. *Astronomy & Astrophysics*, *533*, A29. https://doi.org/10.1051/0004-6361/201117024

Dudok de Wit, T. D., Kopp, G., Frohlich, C., & Scholl, M. (2017). Methodology to create a new total solar irradiance record: Making a composite out of multiple data records. *Geophysical Research Letters*, *44*(3), 1196–1203. https://doi.org/10.1002/2016gl071866

Egorova, T., Rozanov, E., Manzini, E., Haberreiter, M., Schmutz, W., Zubov, V., & Peter, T. (2004). Chemical and dynamical response to the 11-year variability of the solar irradiance simulated with a chemistry-climate model. *Geophysical Research Letters*, *31*, L06119. https://doi.org/10.1029/2003gl019294

Ermolli, I., Matthes, K., Dudok de Wit, T., Krivova, N. A., Tourpali, K., Weber, M., et al. (2013). Recent variability of the solar spectral irradiance and its impact on climate modelling. *Atmospheric Chemistry and Physics*, *13*(8), 3945–3977. https://doi.org/10.5194/acp-13-3945-2013

Fligge, M., & Solanki, S. K. (1997). Inter-cycle variations of solar irradiance: Sunspot areas as a pointer. *Solar Physics*, *173*(2), 427–439. https://doi.org/10.1023/A:1004971807172

Foukal, P., & Lean, J. (1986). The influence of faculae on total solar irradiance and luminosity. *Astrophysical Journal*, *302*(2), 826–835. https://doi.org/10.1086/164043

Frohlich, C. (2006a). Solar irradiance variability since 1978. *Solar Variability and Earth's Climate*, *76*(4), 731–734. https://doi.org/10.1007/s11214-006-9046-5

Frohlich, C. (2006b). Solar irradiance variability since 1978—Revision of the PMOD composite during solar cycle 21. *Space Science Reviews*, *125*(1-4), 53–65. https://doi.org/10.1007/s11214-006-9046-5

Frohlich, C., & Lean, J. (1998). The Sun's total irradiance: Cycles, trends and related climate change uncertainties since 1976. *Geophysical Research Letters*, *25*(23), 4377–4380. https://doi.org/10.1029/1998gl900157

Frohlich, C., & Lean, J. (2004). Solar radiative output and its variability: Evidence and mechanisms. *Astronomy and Astrophysics Review*, *12*(4), 273–320. https://doi.org/10.1007/s00159-004-0024-1

Gueymard, C. A., Myers, D., & Emery, K. (2002). Proposed reference irradiance spectra for solar energy systems testing. *Solar Energy*, *73*(6), 443–467. https://doi.org/10.1016/S0038-092x(03)00005-7

Gyori, L., Baranyi, T., & Ludmany, A. (2011). Photospheric data programs at the Debrecen Observatory. *Proceedings of the International Astronomical Union*, *6*(Symp. S273), 5. https://doi.org/10.1017/S174392131101564X

Haberreiter, M., Scholl, M., Dudok de Wit, T., Kretzschmar, M., Misios, S., Tourpali, K., & Schmutz, W. (2017). A new observational solar irradiance composite. *Journal of Geophysical Research: Space Physics*, *122*, 5910–5930. https://doi.org/10.1002/2016ja023492

Harder, J., Lawrence, G., Fontenla, J., Rottman, G., & Woods, T. (2005). The spectral irradiance monitor: Scientific requirements, instrument design, and operation modes. *Solar Physics*, *230*(1-2), 141–167. https://doi.org/10.1007/s11207-005-5007-5

Harder, J. W., Fontenla, J. M., Pilewskie, P., Richard, E. C., & Woods, T. N. (2009). Trends in solar spectral irradiance variability in the visible and infrared. *Geophysical Research Letters*, *36*, L07801. https://doi.org/10.1029/2008gl036797

Harder, J. W., Beland, S., & Snow, M. (2019). SORCE-based Solar Spectral Irradiance (SSI) record for input into chemistry climate studies https://doi.org/doi:10.1029/2019EA000737

Hathaway, D. H. (2010). The solar cycle. *Living Reviews in Solar Physics*, *7*(1). https://doi.org/10.12942/lrsp-2010-1

Hathaway, D. H., Wilson, R. M., & Reichmann, E. J. (2002). Group sunspot numbers: Sunspot cycle characteristics. *Solar Physics*, *211*(1-2), 357–370. https://doi.org/10.1023/A:1022425402664

Horne, J. H., & Baliunas, S. L. (1986). A prescription for period analysis of unevenly sampled time-series. *Astrophysical Journal*, *302*(2), 757–763. https://doi.org/10.1086/164037

Hoyt, D. V., & Schatten, K. H. (1998). Group sunspot numbers: A new solar activity reconstruction. *Solar Physics*, *181*(2), 491–512. https://doi.org/10.1023/A:1005056326158

Hunter, L., Baltzer, T., Wilson, A., Lindholm, D., Snow, M., Woodraska, D., et al. (2018). *LASP interactive solar irradiance datacenter (LISIRD), Paper presented at the American Geophysical Union*. Washington, D. C., USA.

Keil, S. L., Henry, T. W., & Fleck, B. (1998). NSO/AFRL/Sac peak K-line monitoring program. *Synoptic Solar Physics*, *140*, 301–309.

Kopp, G. (2014). An assessment of the solar irradiance record for climate studies. *Journal of Space Weather and Space Climate*, *4*, A14. https://doi.org/10.1051/swsc/2014012

Kopp, G., & Lawrence, G. (2005). The total irradiance monitor (TIM): Instrument design. *Solar Physics*, *230*(1-2), 91–109. https://doi.org/10.1007/s11207-005-7446-4

Kopp, G., Lawrence, G., & Rottman, G. (2005). The total irradiance monitor (TIM): Science results. *Solar Physics*, *230*(1-2), 129–139. https://doi.org/10.1007/s11207-005-7433-9

Kopp, G., & Lean, J. (2013). *The solar climate data record: Scientific assessment of strategies to mitigate an impending gap in total solar irradiance observations between the NASA SORCE and NOAA TSIS missions (Study B). Prepared for NOAA's National Climatic Data Center (NCDC)*. NC. Retrieved from https://www.nap.edu/read/18371/chapter/7#75

Kopp, G., & Lean, J. L. (2011). A new, lower value of total solar irradiance: Evidence and climate significance. *Geophysical Research Letters*, *38*, L01706. https://doi.org/10.1029/2010gl045777

Kren, A. C., Pilewskie, P., & Coddington, O. (2017). Where does Earth's atmosphere get its energy? *Journal of Space Weather and Space Climate*, *7*, A10. https://doi.org/10.1051/swsc/2017007

Krivova, N. A., Solanki, S. K., & Floyd, L. (2006). Reconstruction of solar UV irradiance in cycle 23. *Astronomy & Astrophysics*, *452*(2), 631–639. https://doi.org/10.1051/0004-6361:200564809

Krivova, N. A., Vieira, L. E. A., & Solanki, S. K. (2010). Reconstruction of solar spectral irradiance since the Maunder minimum. *Journal of Geophysical Research, Space Physics*, *115*, A12112. https://doi.org/10.1029/2010ja015431

Kurucz, R. L. (1991). New opacity calculations. *Stellar Atmospheres: Beyond Classical Models*, *341*, 441–448. https://doi.org/10.1007/978-94-011-3554-2_42

Lean, J. (2000). Evolution of the sun's spectral irradiance since the Maunder minimum. *Geophysical Research Letters*, *27*(16), 2425–2428. https://doi.org/10.1029/2000gl000043

Lean, J., Cook, J., Marquette, W., & Johannesson, A. (1998). Magnetic sources of the solar irradiance cycle. *Astrophysical Journal*, *492*(1), 390–401. https://doi.org/10.1086/305015

Lean, J., Rottman, G., Harder, J., & Kopp, G. (2005). SORCE contributions to new understanding of global change and solar variability. *Solar Physics*, *230*(1-2), 27–53. https://doi.org/10.1007/s11207-005-1527-2

Lean, J., White, O. R., Livingston, W. C., & Picone, J. M. (2001). Variability of a composite chromospheric irradiance index during the 11-year activity cycle and over longer time periods. *Journal of Geophysical Research, Space Physics*, *106*(A6), 10645–10658. https://doi.org/10.1029/2000ja000340

Lean, J., & Woods, T. (2010). Solar spectral irradiance measurements and models. In K. Schrijver & G. Siscoe (Eds.), *Evolving Solar Physics and the Climates of Earth and Space* (Chap. 10, pp. 269–298). Cambridge University Press.

Lean, J. L. (2018). Estimating solar irradiance since 850 CE. *Earth and Space Science*, *5*(4), 133–149. https://doi.org/10.1002/2017ea000357

Lean, J. L., & DeLand, M. T. (2012). How does the Sun's spectrum vary? *Journal of Climate*, *25*(7), 2555–2560. https://doi.org/10.1175/Jcli-D-11-00571.1

Levelt, P. F., Joiner, J., Tamminen, J., Veefkind, J. P., Bhartia, P. K., Zweers, D. C. S., et al. (2018). The ozone monitoring instrument: Overview of 14 years in space. *Atmospheric Chemistry and Physics*, *18*(8), 5699–5745. https://doi.org/10.5194/acp-18-5699-2018

Machol, J., Snow, M., Woodraska, D., Woods, T.,Viereck, R., & Coddington, O. (2019). An Improved Lyman-alpha Composite. *Earth and Space Science* https://doi.org/doi:10.1029/2019EA000648

Marchenko, S. V., & DeLand, M. T. (2014). Solar spectral irradiance changes during cycle 24. *Astrophysical Journal*, *789*(2), 117. https://doi.org/10.1088/0004-637x/789/2/117

Marchenko, S. V., Woods, T.N., DeLand, M. T., Mauceri, S., Pilewskie, P., & Haberreiter, M. (2019). Improved Aura/OMI Solar Spectral Irradiance: Comparisons with Independent Datasets and Model Predictions. *Earth and Space Science*. https://doi.org/0.1029/2019EA000624

Matthes, K., Funke, B., Andersson, M. E., Barnard, L., Beer, J., Charbonneau, P., et al. (2017). Solar forcing for CMIP6 (v3.2). *Geoscientific Model Development*, *10*(6), 2247–2302. https://doi.org/10.5194/gmd-10-2247-2017

Mauceri, S., Pilewskie, P., Richard, E., Coddington, O., Harder, J., & Woods, T. (2018). Revision of the Sun's spectral irradiance as measured by SORCE SIM. *Solar Physics*, *293*(12), 161. https://doi.org/10.1007/s11207-018-1379-1

McClintock, W. E., Rottman, G. J., & Woods, T. N. (2005). Solar-stellar irradiance comparison experiment II (SOLSTICE II): Instrument concept and design. *Solar Physics*, *230*(1-2), 225–258. https://doi.org/10.1007/s11207-005-7432-x

McComas, I., & Coddington, O. (2018). *The sensitivity of empirical regression models of solar irradiance to underlying methodology*. Washington, DC USA: Paper presented at the American Geophysical Union.

Meftah, M., Bolsée, D., Damé, L., Hauchecorne, A., Pereira, N., Irbah, A., et al. (2016). Solar irradiance from 165 to 400 nm in 2008 and UV variations in three spectral bands during solar cycle 24. *Solar Physics*, *291*(12), 3527–3547. https://doi.org/10.1007/s11207-016-0997-8

NRC (2004). *Climate data records from environmental satellites: Interim report*. Washington, DC: National Academies Press.

Richard, E. C., Harber, D., Rutkowski, J., Drake, G., Harder, J., Pilewskie, P., et al. (2011). *Future long-term measurements of solar spectral irradiance by the TSIS spectral irradiance monitors: Improvements in measurement accuracy and stability*. Paper presented at the 11th International Conference on New Developments and Applications in Optical Radiometry. Maui, HI: NEWRAD.

Richard, E. C., Harber, D., Rutkowski, J., Triplett, M., Pilewskie, P., Brown, S., & Lykke, K. (2014). *The future of solar spectral irradiance measurements from space: ISS TSIS and beyond*. Paris, France: Paper presented at the Solar Metrology, Needs and Methods Symposium.

Rottman, G. (2005). The SORCE mission. *Solar Physics*, *230*(1-2), 7–25. https://doi.org/10.1007/s11207-005-8112-6

Schimel, D., Alves, D., Enting, I., Heimann, M., Joos, F., Raynaud, D., . . . Wuebbles, D. (1996). *Radiative Forcing of Climate Change*. Retrieved from https://www.ipcc.ch/reports/

Schmidt, G. A., Jungclaus, J. H., Ammann, C. M., Bard, E., Braconnot, P., Crowley, T. J., et al. (2011). Climate forcing reconstructions for use in PMIP simulations of the last millennium (v1.0). *Geoscientific Model Development*, *4*(1), 33–45. https://doi.org/10.5194/gmd-4-33-2011

Shine, K. P., Derwent, R. G., Wuebbles, D. J., & Morcrette, J.-J. (1990). *Climate change—The IPCC scientific assessment*. Retrieved from https://www.ipcc.ch/reports/

Snow, M., McClintock, W. E., Rottman, G., & Woods, T. N. (2005). Solar-stellar irradiance comparison experiment II (SOLSTICE II): Examination of the solar-stellar comparison technique. *Solar Physics*, *230*(1-2), 295–324. https://doi.org/10.1007/s11207-005-8763-3

Snow, M., McClintock, W. E., & Woods, T. N. (2010). Solar spectral irradiance variability in the ultraviolet from SORCE and UARS SOLSTICE. *Advances in Space Research*, *46*(3), 296–302. https://doi.org/10.1016/j.asr.2010.03.027

Snow, M., McClintock, W. E., Woods, T. N., White, O. R., Harder, J. W., & Rottman, G. (2005). The MgII index from SORCE. *Solar Physics*, *230*(1-2), 325–344. https://doi.org/10.1007/s11207-005-6879-0

Snow, M., Weber, M., Machol, J., Viereck, R., & Richard, E. (2014). Comparison of magnesium II core-to-wing ratio observations during solar minimum 23/24. *Journal of Space Weather and Space Climate*, *4*, A04. https://doi.org/10.1051/swsc/2014001

Solomon, S., Qin, D., Manning, M., Chen, Z., Marquis, M., Averyt, K. B., . . . Miller, H. L. (2007). *IPCC, climate change 2007: The physical science basis, contribution of working group I to the fourth assessment report of the integovernmental panel on climate change*. Retrieved from https://www.ipcc.ch/report/ar4/wg1/

Steinegger, M., Brandt, P. N., & Haupt, H. F. (1996). Sunspot irradiance deficit, facular excess, and the energy balance of solar active regions. *Astronomy & Astrophysics*, *310*(2), 635–645.

Stephens, G. L., Li, J., Wild, M., Clayson, C. A., Loeb, N., Kato, S., et al. (2012). An update on Earth's energy balance in light of the latest global observations. *Nature Geoscience*, *5*(10), 691–696. https://doi.org/10.1038/Ngeo1580

Swartz, W. H., Stolarski, R. S., Oman, L. D., Fleming, E. L., & Jackman, C. H. (2012). Middle atmosphere response to different descriptions of the 11-yr solar cycle in spectral irradiance in a chemistry-climate model. *Atmospheric Chemistry and Physics*, *12*(13), 5937–5948. https://doi.org/10.5194/acp-12-5937-2012

Tapping, K. F. (2013). The 10.7 cm solar radio flux (F-10.7). *Space Weather-the International Journal of Research and Applications*, *11*(7), 394–406. https://doi.org/10.1002/swe.20064

Thuillier, G., Herse, M., Simon, P. C., Labs, D., Mandel, H., Gillotay, D., & Foujols, T. (1998). The visible solar spectral irradiance from 350 to 850 nm as measured by the SOLSPEC spectrometer during the ATLAS I mission. *Solar Physics*, *177*(1-2), 41–61. https://doi.org/10.1023/A:1004953215589

Unruh, Y. C., Solanki, S. K., & Fligge, M. (1999). The spectral dependence of facular contrast and solar irradiance variations. *Astronomy & Astrophysics*, *345*(2), 635–642.

Viereck, R., Puga, L., McMullin, D., Judge, D., Weber, M., & Tobiska, W. K. (2001). The MgII Index: A proxy for solar EUV. *Geophysical Research Letters*, *28*(7), 1343–1346. https://doi.org/10.1029/2000gl012551

Wang, Y. M., Lean, J. L., & Sheeley, N. R. (2005). Modeling the sun's magnetic field and irradiance since 1713. *Astrophysical Journal*, *625*(1), 522–538. https://doi.org/10.1086/429689

Wang, Y. M., & Sheeley, N. R. (2015). Coronal mass ejections and the solar cycle variation of the Sun's open flux. *Astrophysical Journal Letters*, *809*(2), L24. https://doi.org/10.1088/2041-8205/809/2/L24

Willson, R. C., & Mordvinov, A. V. (2003). Secular total solar irradiance trend during solar cycles 21-23. *Geophysical Research Letters*, *30* L16038(5), 1199. https://doi.org/10.1029/2002gl016038

Woods, T. N., Chamberlin, P. C., Harder, J. W., Hock, R. A., Snow, M., Eparvier, F. G., et al. (2009). Solar irradiance reference spectra (SIRS) for the 2008 whole heliosphere interval (WHI). *Geophysical Research Letters*, *36*, L01101. https://doi.org/10.1029/2008gl036373

Woods, T. N., Eparvier, F. G., Harder, J., & Snow, M. (2018). Decoupling solar variability and instrument trends using the multiple same-irradiance-level (MuSIL) analysis technique. *Solar Physics*, *293*(5), 76. https://doi.org/10.1007/s11207-018-1294-5

Woods, T. N., & Rottman, G. (2005). XUV photometer system (XPS): Solar variations during the SORCE mission. *Solar Physics*, *230*(1-2), 375–387. https://doi.org/10.1007/s11207-005-2555-7

Yeo, K. L., Krivova, N. A., & Solanki, S. K. (2017). EMPIRE: A robust empirical reconstruction of solar irradiance variability. *Journal of Geophysical Research: Space Physics*, *122*, 3888–3914. https://doi.org/10.1002/2016ja023733

Yeo, K. L., Krivova, N. A., Solanki, S. K., & Glassmeier, K. H. (2014). Reconstruction of total and spectral solar irradiance from 1974 to 2013 based on KPVT, SoHO/MDI, and SDO/HMI observations. *Astronomy & Astrophysics*, *570*, A85. https://doi.org/10.1051/0004-6361/201423628

Yeo, K. L., Solanki, S. K., Norris, C. M., Beeck, B., Unruh, Y. C., & Krivova, N. A. (2017). Solar irradiance variability is caused by the magnetic activity on the solar surface (vol 119, 091102, 2017). *Physical Review Letters*, *119*(13), 139902. https://doi.org/10.1103/PhysRevLett.119.139902